Functional brain defects in a mouse model of a chromosomal t(1;11) translocation that disrupts DISC1 and confers increased risk of psychiatric illness

Functional brain defects in a mouse model of a chromosomal t(1;11) translocation that disrupts *DISC1* and confers increased risk of psychiatric illness

Marion Bonneau[1], Shane T. O'Sullivan[1], Miguel A. Gonzalez-Lozano[2], Paul Baxter[3], Phillippe Gautier[4], Elena Marchisella[5], Neil R. Hardingham[6], Robert A. Chesters[7], Helen Torrance[1], David M. Howard[8, 9], Maurits A. Jansen[10], Melanie McMillan[11], Yasmin Singh[12], Michel Didier[13], Frank Koopmans[2], Colin A. Semple[4], Andrew M. McIntosh[9], Hansjürgen Volkmer[14], Maarten Loos[5], Kevin Fox[6], Giles E. Hardingham[3], Anthony C. Vernon[7, 15], David J. Porteous[1], August B. Smit[2], David J. Price[3], J. Kirsty Millar[1]*

[1]Centre for Genomic and Experimental Medicine, MRC Institute of Genetics and Molecular Medicine at the University of Edinburgh, Edinburgh, UK

[2]Department of Molecular and Cellular Neurobiology, Center for Neurogenomics and Cognitive Research, VU University, Amsterdam, The Netherlands

[3]Centre for Discovery Brain Sciences, Hugh Robson Building, The University of Edinburgh, Edinburgh, UK

[4]MRC Human Genetics Unit, MRC Institute of Genetics and Molecular Medicine at the University of Edinburgh, Edinburgh, UK

[5]Sylics Synaptologics BV, Amsterdam, The Netherlands

[6]School of Biosciences, Museum Avenue, Cardiff University, Cardiff, UK

[7]Department of Basic and Clinical Neuroscience, Institute of Psychiatry, Psychology and Neuroscience, King's College London, London, UK

[8]Social, Genetic and Developmental Psychiatry Centre, Institute of Psychiatry, Psychology & Neuroscience, King's College London, UK

[9]Division of Psychiatry, Kennedy Tower, The University of Edinburgh, Edinburgh, UK

[10]Edinburgh Preclinical Imaging, The Chancellor's Building, The University of Edinburgh, Edinburgh, UK,

[11]Centre for Reproductive Health, The Queen's Medical Research Institute, The University of Edinburgh, Edinburgh, UK

[12]Centre for Genomics and Transcriptomics, Paul-Ehrlich-Straße 23, Tübingen, Germany

[13]Translational Sciences at Sanofi, Chilly-Mazarin, France

[14]Department of Molecular Biology, NMI Natural and Medical Sciences Institute at the University of Tübingen, Reutlingen, Germany

[15]MRC Centre for Neurodevelopmental Disorders, King's College London, London, UK

*Corresponding author

Tel: +44 (0)131 651 8732

Fax: +44 (0)131 651 1059

Email: kirsty.millar@igmm.ed.ac.uk

Address: Centre for Genomic and Experimental Medicine, MRC Institute of Genetics and Molecular Medicine at the University of Edinburgh, Crewe Road, Edinburgh, EH4 2XU, UK

Running title: t(1;11) mouse model

Abstract

A balanced t(1;11) translocation that directly disrupts *DISC1* is linked to schizophrenia and affective disorders. We previously showed that a mutant mouse, named *Der1*, recapitulates the effect of the translocation upon DISC1 expression. Here, RNAseq analysis of *Der1* mouse brain tissue found enrichment for dysregulation of the same genes and molecular pathways as in neuron cultures generated previously from human t(1;11) translocation carriers via the induced pluripotent stem cell route. *DISC1* disruption therefore apparently accounts for a substantial proportion of the effects of the t(1;11) translocation. RNAseq and pathway analysis of the mutant mouse predict multiple *Der1*-induced alterations converging upon synapse function and plasticity. Synaptosome proteomics confirmed that the *Der1* mutation impacts synapse composition, and electrophysiology found reduced AMPA:NMDA ratio in hippocampal neurons, indicating changed excitatory signalling. Moreover, hippocampal Parvalbumin-positive interneuron density is increased, suggesting that the *Der1* mutation affects inhibitory control of neuronal circuits. These phenotypes predict that neurotransmission is impacted at many levels by *DISC1* disruption in human t(1;11) translocation carriers. Notably, genes implicated in schizophrenia, depression and bipolar disorder by large-scale genetic studies are enriched among the *Der1*-dysregulated genes, just as we previously observed for the t(1;11) translocation carrier-derived neurons. Furthermore, RNAseq analysis predicts that the *Der1* mutation primarily targets a subset of cell types, pyramidal neurons and interneurons, previously shown to be vulnerable to the effects of common schizophrenia-associated genetic variants. In conclusion, DISC1 disruption by the t(1;11) translocation may contribute to the psychiatric disorders of translocation carriers through commonly affected pathways and processes in neurotransmission.

Introduction

Psychiatric illnesses such as schizophrenia and recurrent affective disorders have a substantial underlying genetic component. Considerable progress has been made in recent years towards identification of the multitude of genes involved using large-scale studies of genome-wide association (GWAS) and recurrent copy number variants (CNVs)[1-6]. GWAS tends to identify genomic loci with common, but small, individual effects that encompass several genes, leaving the specific causal genes unidentified, unless further refinements are applied. In contrast, recurrent CNVs are rare, tending to exert a strong effect (most likely due to large changes in expression levels of the genes at fault), but also usually encompass multiple genes. Chromosomal rearrangements, such as translocations, linked to psychiatric disorders are rarer still, but can have the advantage of strong effects and accurate pinpointing of genes due to their disruption by the breakpoints of the rearranged genomic segments. It is likely that convergence of data arising from genomic events such as these will assist in revealing the genes and mechanisms that predispose to major mental illness.

One example of a chromosomal rearrangement linked to psychiatric disorders is a t(1;11) translocation that substantially increases risk of developing schizophrenia or affective disorders in a large Scottish family[7-9]. The psychiatric symptoms presented by t(1;11) translocation carriers are typical, that is, they are within the range of current diagnostic criteria, and are accompanied by reduced white matter integrity[10], cortical thickness[11] and prefrontal cortex gyrification[9], all typical of schizophrenia. Carriers of the t(1;11) translocation also have decreased glutamate levels in the dorsolateral prefrontal cortex[9]. Moreover, transcriptome analysis of induced pluripotent stem cell (IPSC)-derived cortical neurons from t(1;11) translocation carriers[12] found enrichment for dysregulated genes at putative schizophrenia and depression loci discovered through large scale GWAS and CNV studies[1-3], potentially identifying some of the genes of interest at those loci, and indicating that the t(1;11) translocation may trigger disease pathways shared with schizophrenic patients who are not translocation carriers.

The t(1;11) translocation directly disrupts the *DISC1* gene on chromosome 1[13]. *DISC1* encodes a potential molecular scaffold protein involved in multiple critical functions in the developing and adult brain[14, 15], including neurogenesis[16-18], neuronal cargo trafficking[19-23] and neurotransmission[23-26]. *DISC1* disruption is therefore likely to contribute substantially to mechanisms leading to psychiatric illness in t(1;11) translocation carriers.

Two apparently non-coding genes of unknown function, *DISC2* and *DISC1FP1* (otherwise known as *Boymaw*), are also disrupted on chromosomes 1 and 11, respectively[13, 27], and potential genetic modifier loci have been identified within the family[28], all of which may additionally impact disease mechanisms in t(1;11) translocation carriers. It is now important to discover how each of these disruptions and putative modifiers relate to the gene expression changes, brain structure alterations and psychiatric symptoms of t(1;11) translocation carriers.

To examine the impact of *DISC1* disruption in isolation from the additional complexities of *DISC2* disruption and loss of normal *DISC1FP1* function, and of potential genetic modifiers, we have utilised a mutant mouse which accurately recapitulates the effects of the translocation upon DISC1 expression[12]. IPSC-derived neural precursor cells and cortical neurons from t(1;11) translocation carriers exhibit reduced *DISC1* expression[12]. Chimeric transcripts encoding aberrant C-terminally truncated chimeric forms of DISC1 are also produced in the IPSC-derived neural cells as a result of fusion between the *DISC1* and *DISC1FP1* genes on the derived chromosome 1[12, 29]. The mutant mouse was precisely engineered to mimic the fusion between *DISC1* and *DISC1FP1* on the derived 1 chromosome and exhibits reduced Disc1 levels plus chimeric transcript expression[12]. This mutant mouse is referred to as *Der1*.

Heterozygous *Der1* mice express reduced levels of wild-type Disc1 plus the aberrant chimeric transcripts[12, 29]. Because Disc1 multimerises[30], there is thus potential in heterozygotes for dominant-negative effects due to interaction between wild-type and mutant Disc1. Homozygotes, however, lack any wild-type Disc1 and may express high levels of aberrant Disc1. Despite heterozygotes corresponding most closely to t(1:11) translocation

carriers, we opted to study both mutant genotypes in order to obtain the most complete understanding of the likely effects of DISC1 disruption. A flow chart (Supplementary Figure 1) illustrates the experimental approach taken, with the aim of allowing the results described here to be compared with previously published t(1:11) translocation studies and integrated with psychiatric genetic association studies of single nucleotide polymorphism (SNP) and CNV variants in the general population. We combine magnetic resonance imaging (MRI), histology, transcriptomics, synaptosome proteomics and electrophysiology to demonstrate that the *Der1* mutation primarily affects cellular properties rather than brain structure, and that it targets a variety of cell types including neurons. Patterns of gene expression and predictions of altered biological processes substantially overlap between *Der1* cortex and IPSC-derived cortical neuron cultures from t(1:11) translocation carriers. We find widespread dysregulation of genes implicated as potential common risk factors for schizophrenia, depression and bipolar disorder. We therefore propose that *DISC1* disruption targets common pathways shared with psychiatric patients who do not carry the t(1;11) translocation, to contribute to the elevated risk of major mental illness displayed by t(1:11) translocation carriers[9].

Materials and methods

Detailed materials and methods are provided in the Supplementary information file.

Results

Adult *Der1* mutant mice show no overt changes in brain structure

Using ex vivo structural MRI, we found no evidence for effects of the *Der1* mutation on overall brain volume or the volumes of 51 brain regions analysed individually (Supplementary Table 1). In the absence of hypotheses arising from the MRI analysis of brain structure, and given that DISC1 is highly expressed in the hippocampus from early development through to adulthood, and that prefrontal cortex (PFC) is affected in t(1:11) translocation carriers[9], these regions were explored in further detail. The *Der1* mutation does

not affect cell densities in the hippocampal Stratum, Radiatum, Lacunosum and Moleculare or prefrontal cortex, nor the thickness of individual cortical layers within the barrel cortex, nor the total cortical thickness in either the barrel cortex or the PFC (Supplementary Figure 2, 3, 4).

RNAseq analysis of adult *Der1* cortex and hippocampus

We next conducted RNASeq using wild-type and heterozygous 'cortex' (consisting of cortices minus hippocampus, cerebellum and olfactory bulbs) and hippocampus. The resulting data were analysed at the whole gene and single exon levels using DESeq2[31] and DEXSeq[32], respectively. Full-length Disc1 expression is reduced in heterozygous *Der1* mouse whole brain as detected by quantitative RT-PCR and immunoblotting[12]. RNAseq also found reduced *Disc1* expression in heterozygous *Der1* cortex and hippocampus (Figure 1a, Supplementary Table 2a, c), confirming the validity of these datasets.

Expression of 30,121 genes was detected in cortex, of which 2,124 and 3,568 are differentially expressed in heterozygotes at the whole gene or exon level respectively (all corrected $p<0.05$, Figure 1b, Supplementary Table 2a, b). Expression of 28,049 genes was detected in hippocampus, of which 175 and 52 are differentially expressed in heterozygotes at the whole gene or exon level respectively (all adjusted $p<0.05$, Supplementary Table 2c, d).

Expression Weighted Cell-type Enrichment (EWCE) analysis of RNASeq data suggests specific cell types are targeted by the *Der1* mutation

EWCE analysis[33] was used to look for evidence that certain cell types are especially vulnerable to the *Der1* mutation. We utilised gene expression profiles generated by hierarchical clustering of single cell RNASeq profiles from 9,970 mouse brain cells and around 15,000 of the most abundantly expressed genes, resulting in 24 cell classes, referred to as the KI Superset[34]. The authors of that study calculated 'specificity values' for each gene within each cell class, to indicate enrichment for expression of that gene in a cell class

compared to the other classes in the Superset[34]. EWCE analysis was used here to determine whether there is enrichment for *Der1*-induced dysregulation of genes with high specificity values for Superset cell classes in cortex (Figure 1c). Statistical significance was observed for pyramidal neurons ('pyramidal somatosensory', 'pyramidal CA1' [which also encompasses neurons from CA2 and the subiculum[34]]), interneurons ('cortical interneuron', 'striatal interneuron'), dopaminergic neurons ('dopaminergic adult neurons', 'hypothalamic dopaminergic neurons'), 'oxytocin/vasopressin-expressing neurons' and 'astrocytes/ependymocytes'. *Der1* hippocampus dysregulated genes are also highly enriched in several cell classes (Figure 1d). Of these, pyramidal neurons ('pyramidal somatosensory'), 'medium spiny neuron' and 'interneuron' achieved statistical significance. 'Pyramidal CA1' reached initial significance in *Der1* hippocampus, but did not survive multiple testing correction. Pyramidal CA1, pyramidal somatosensory and medium spiny neurons should reside primarily in the hippocampus, cortex and striatum, respectively, thus some of these findings were initially unexpected. However, the previously published hierarchical clustering of cell classes[34] indicated that 'pyramidal CA1' and 'pyramidal somatosensory' are highly similar, with medium spiny neurons the next most closely related cell type. We therefore infer that in cortex and hippocampus the *Der1* mutation may target general features shared between these three neuron classes.

Based on these findings, Parvalbumin-expressing interneuron density was quantified in adult PFC and hippocampus. PFC shows no change (Supplementary Figure 5), however there is a trend towards an increase in the dentate gyrus (p=0.07), and a significant increase in *Der1* heterozygotes when the whole hippocampus is examined (34% increase, Figure 1e, f). The EWCE analysis data pointing to hippocampal interneuron targeting could therefore be due, at least partially, to increased density of interneurons expressing Parvalbumin at high levels. This contrasts with previous reports of reduced Parvalbumin-positive cell density in mice expressing mutant DISC1, or in response to endogenous Disc1 knockdown[35].

We also hypothesised that the cell types most affected by the *Der1* mutation might be susceptible to apoptosis, as quantified using Activated-Caspase-3. Of the adult PFC and

hippocampal regions examined, there is a trend towards increased apoptosis in CA1 (p=0.06, Supplementary Figure 6), which may indicate that CA1 cells are particularly vulnerable. This could lead to reduced cell density in CA1, a parameter that unfortunately could not be adequately examined due to the prohibitively tight packing of cells in this region.

RNASeq deconvolution suggests that cell class proportions are unaltered by the *Der1* mutation

RNASeq deconvolution was carried out utilising gene expression data (rather than the specificity values used above for EWCE analysis) for the most highly enriched genes from the 24 cell classes of the Superset[34]. First, the ability of the deconvolution programme, CIBERSORT[36], to deconvolve the 24 cell classes was examined by generating artificial *in silico* samples with varying proportions of each cell class (Supplementary Figure 7). Using two specificity value thresholds, CIBERSORT was able to deconvolve most cell types. The exceptions include embryonic cell types, which should be absent from our *Der1* samples, and rarer cell types in adult brain such as neural progenitors and neuroblasts. When used to deconvolve *Der1* cortex and hippocampus whole gene DESeq2 RNASeq data, CIBERSORT found no evidence for an effect of the mutation upon the relative proportion of any of the cell classes examined (Supplementary Figure 8). The increased density of hippocampal Parvalbumin-positive interneurons (Figure 1e, f) therefore may not represent a general effect upon all hippocampal interneuron types. Likewise, the trend towards increased hippocampal CA1 apoptosis (Supplementary Figure 6) does not translate to a detectably decreased density of pyramidal CA1 neurons, possibly because this Superset class also contains pyramidal neurons from CA2 and the subiculum[34].

Molecular pathway analysis predicts wide-ranging effects of the *Der1* mutation

Since the patterns of gene dysregulation are not explained by overtly altered cell proportions, the RNASeq data were next used to predict effects upon canonical pathways. Ingenuity Pathway Analysis (IPA), an unbiased method for examining transcriptomic data

using statistical significance and magnitude plus direction of fold-change, was carried out using the whole gene level DESeq2 data, or combined DESeq2 plus exon level DEXSeq data. This analysis predicts effects upon diverse pathways including metabolic, stress-response and important neurosignalling processes (Figure 2a). A selection of these pathways, based on statistical significance or relevance to later parts of this study, are discussed below.

Mitochondrial dysfunction, including increased oxidative phosphorylation is strongly predicted, based largely upon upregulated whole gene expression of multiple complex I, III and IV components (Supplementary Figure 9), consistent with DISC1's known role in regulating oxidative phosphorylation[37, 38]. Moreover, the chimeric transcripts expressed by *Der1* mice encode aberrant mitochondrial species that induce mitochondrial dysfunction[29].

Also upregulated at the whole gene level is the mitochondrial pathway 'Fatty acid β-oxidation I' (Supplementary Figure 10) which degrades fatty acids to release energy. Dysregulated enzymes feeding into this pathway are involved in fatty acid synthesis and break down. Together these changes imply altered levels of lipids, which are critical for many brain processes.

The 'CREB signalling in neurons' pathway (Figure 2b) is activated by cell surface glutamate receptors, including AMPA and NMDA receptors, and calcium channels. It regulates gene expression changes that are critical for synaptic plasticity and long-term potentiation (LTP), both known to be DISC1-modulated[30]. DISC1 is also already known to regulate CREB signalling[30], and in our study IPA predicts that downregulation of Creb1 activity is responsible for many of the gene expression changes (p=9e-9, z=-3). Indeed, there is enrichment (hypergeometric p=0.02) for dysregulation of genes containing conserved cAMP-Response Elements (CREs, http://natural.salk.edu/creb/, Supplementary Table 3) in heterozygous *Der1* cortex, with 203 (9.6%) of the genes dysregulated at the whole gene level having CREs. The *Der1* mutation potentially affects activation of the pathway via AMPA receptor subunit degradation[39], and NMDA receptor membrane dynamics and surface expression[12]. Moreover, genes encoding glutamate receptors,

265 including AMPA and NMDA receptor subunits, and several synaptic scaffolds are
266 dysregulated (Figure 2b).
267 Using the combined dysregulated DESeq2 plus DEXSeq data, IPA also determined
268 that many cellular functions are enriched for differentially expressed genes (Table 1,
269 Supplementary Table 4a). Predictions relating to neurotransmission, synaptic plasticity and
270 LTP are related to the 'CREB signalling in neurons' pathway above, plus genes encoding
271 inhibitory signalling factors, such as subunits of $GABA_A$ and $GABA_B$ receptors. Predictions
272 relating to vesicle transport and exo/endocytosis are based on dysregulated genes encoding
273 vesicle trafficking factors; voltage-gated calcium channel subunits as well as synaptotagmins
274 and syntaxins that together mediate calcium-dependent neurotransmitter release;
275 components of the exocyst complex; and components of the endocytic Clathrin-associated-
276 Adaptor-Protein-Complex. The wide-ranging neuronal morphology and cytoskeleton-related
277 predictions are based on multiple genes involved in diverse relevant processes. Similarly,
278 the cell-cell contact/adhesion-related functions are widespread, but notably encompass
279 genes required for early synapse formation, such as latrophilins, as well as maintenance of
280 trans-synaptic connections, for example neuroligins and neurexins. Other predictions relate
281 to cell proliferation, neuronal migration and circadian rhythms. All of these processes are
282 already known to involve DISC1[12, 16, 18, 21, 25, 35, 40-43].
283 *Der1* hippocampus RNASeq data were similarly analysed. IPA did not strongly
284 predict any canonical pathway changes due to the relatively small number of changes, but
285 did predict altered functions that largely reflect those for cortex (Supplementary Table 4b, 5),
286 and there is enrichment for dysregulation of 86 shared genes (39% of the total dysregulated
287 hippocampal genes, Supplementary Table 2c, d) in both regions (p=7e-11). Myelination is
288 also predicted to be affected, consistent with previous studies demonstrating DISC1
289 involvement in oligodendrocyte differentiation and function[44-46].
290 Numerous processes are thus predicted to be affected by the *Der1* mutation in cortex
291 and hippocampus, with striking convergence upon neurotransmission.
292

Molecular pathway analysis of targeted cell types identified by EWCE analysis

EWCE analysis identified cell classes that may be targeted by the *Der1* mutation (Figure 1c, d). We reasoned that the cell class-enriched gene expression changes may inform on the impact of the *Der1* mutation in each cell type. Pathway analysis was therefore carried out using the cell class-enriched dysregulated genes (Supplementary Table 6, 4c). *Der1* cortex pyramidal neuron (CA1 and somatosensory) and interneuron terms relate to synaptic transmission. *Der1* cortex astrocyte/ependymocyte terms relate to lipid metabolism and uptake of glutamine/glutamate. The lipid metabolism predictions are based on upregulation of genes encoding enzymes involved in fatty acid β-oxidation, and other aspects of brain lipid metabolism. This is related to the *Der1* cortex RNASeq canonical pathway prediction 'Fatty Acid β-oxidation I' (Figure 2a), and indicates a potential imbalance between lipid synthesis and oxidation. Since astrocytes are a major source of brain lipid which is widely utilised, including for synapse function[47] and myelination by oligodendrocytes[48], these processes may be compromised via astrocyte dysfunction. The glutamine/glutamate uptake predictions are based on dysregulated expression of genes such as *Slc1a2,* which encodes the synaptic glutamate transporter Eaat2. Astrocytes are critical regulators of glutamine and glutamate homeostasis in the brain, which includes glutamate clearance from synapses, and consequent regulation of glutamatergic neurotransmission and synaptic plasticity[49]. There were no convincing findings for the other cell classes examined.

Shared gene dysregulation in heterozygous *Der1* cortex and t(1:11) translocation carrier-derived cortical neuron cultures confirms the relevance of the *Der1* RNASeq findings to psychiatric illness

To determine how the above RNASeq data analyses of the *Der1* mouse relate to the t(1:11) translocation, we compared the *Der1* mouse data to previously published RNASeq data generated from t(1:11) translocation carrier-derived neuron cultures[12]. Human IPSC-derived neurons grown in culture are not directly comparable to adult mouse brain tissue. Even so, a

trend towards enrichment for shared gene expression changes was evident from the 20 dysregulated genes in common between IPSC-derived cortical neuron cultures from t(1:11) translocation carriers[12] and heterozygous *Der1* hippocampus (p=0.06, Supplementary Table 2c, d), while 511 genes are differentially expressed in both heterozygous *Der1* mouse cortex and the IPSC-derived cortical neuron cultures (Supplementary Table 2a, b), demonstrating significant enrichment (p=1e-14), and further validating the *Der1* mouse as an accurate model for the effect of the t(1:11) translocation upon DISC1 expression. An overlapping set of cellular functions were also identified in the human cortical neuron cultures and heterozygous *Der1* mouse cortex (Table 1, Supplementary Table 4a, d). Moreover, for most of the shared functions there is either significant enrichment or a trend towards enrichment for a common set of differentially expressed genes (Table 1). This convergence indicates that disruption of *DISC1* likely contributes substantially to the altered molecular pathways in the human neuron cultures.

Nonetheless, several functions are enriched in the *Der1* cortex data, but not in the human cortical neuron data. Many relate specifically to synaptic plasticity and LTP, processes that are constitutive in brain, but which require stimulation to be detected in neuronal cultures. A number of other changes relate specifically to development of dendrites, which may not reach maturity in IPSC-derived neuronal cultures[50].

Mass spectrometry and SynGO analysis of adult *Der1* synaptosomes confirm synaptic changes

To complement the RNASeq analysis, synaptosome fractions were prepared from hetero- or homozygous *Der1* mice and mass spectrometry was used to determine whether synaptosomal protein expression profiles differ between mutant and wild-type mice. Of the 2,783 detected proteins in cortex, no changes survived multiple correction testing in synaptosomes prepared from *Der1* mice (Supplementary Table 7a, Supplementary Figure 11). Of the 2,183 proteins detected in hippocampus, 62 were found to be dysregulated in homozygotes (FDR adjusted p-value < 0.05, Supplementary Table 7b, Supplementary

Figure 11). These proteins were annotated to well-established synaptic genes using the SynGO database[51] (Figure 2c, Supplementary Table 7c). This is an expert-curated database of gene ontology terms relating to synapses. From the 62 regulated proteins, 26 were found annotated in SynGO, 24 with cellular component annotation and 19 with biological processes annotation. Dysregulated proteins were found annotated across a wide spectrum of pre- and post-synapse functions. For instance, several proteins were annotated to the postsynaptic density, such as Camk2a (downregulated); AMPA receptor subunits (downregulated); the DISC1 interactor Trio[52], which modulates AMPA receptor currents in hippocampal CA1 pyramidal neurons[53]; vesicle proteins Exoc4, an exocyst component, and the SNARE STX7; and Gad2, a presynaptic protein that synthesises GABA in interneurons. These changes point to effects upon similar synaptic processes to those highlighted by RNASeq analysis. However, fewer changes were detected in the synaptosomes, probably due to the lower number of proteins identified in comparison with the RNASeq analysis, in which many relevant RNASeq changes were detected at the isoform level.

Functional effects of the *Der1* mutation upon synapses

The RNAseq data point towards effects of the *Der1* mutation upon synapses, which was confirmed by subsequent synaptic proteomics analysis. The observed changes include subtly altered expression of NMDA receptor isoforms and reduced AMPA receptor subunit levels. Moreover, we previously demonstrated that cultured hippocampal neuron dynamics and cell surface/synaptic expression of NMDA receptors are dysregulated by the *Der1* mutation[12].

To examine these receptors functionally, whole cell patch-clamping was used to record currents from both receptor types in mature cultured hippocampal neurons (Figure 2d). The AMPA:NMDA ratio is decreased in homozygous *Der1* neurons indicating functional imbalance between these two receptor subtypes. This may be due in part to altered AMPA receptor currents, which although not statistically significant, are decreased in hetero- and homozygous neurons. To discover whether this whole cell patch-clamp finding extends to

receptors located at synapses in heterozygous *Der1* hippocampus, and in cortex, will require future in-depth electrophysiological measurements. If it does indeed extend to synapses, the decreased AMPA:NMDA ratio could have many consequences including impaired triggering of NMDA receptor-dependent LTP, which is initiated by AMPA receptor-induced release of the magnesium block on NMDA receptors.

Enrichment for dysregulation of putative schizophrenia, bipolar disorder and depression risk genes in heterozygous *Der1* cortex and hippocampus

A large number of putative schizophrenia risk genes have been identified from two large-scale GWAS and one large-scale CNV study[1-3]. IPA maps many of these genes to shared molecular pathways. The top canonical pathway (Figure 3a) is 'CREB signalling in neurons'. Others include 'Synaptic long-term potentiation' and 'Synaptic long-term depression', both mechanisms underlying synaptic plasticity. These findings largely agree with previous observations[54].

The heterozygous *Der1* cortex combined RNASeq DESeq2 plus DEXSeq data were compared to the list of putative schizophrenia risk genes used above[1, 2], but including only genes encoding synaptic proteins from the CNV study[3] as defined by its authors. This identified significant enrichment for dysregulation of schizophrenia candidate gene orthologues (Table 2, Supplementary Table 2a, b). The top canonical pathways identified using this set of genes for IPA are 'Synaptic long-term depression', 'CREB signalling in neurons', 'Synaptic long-term potentiation' and 'Calcium signalling' (Figure 3a-c). These predictions are among the top five of those obtained using the full set of putative schizophrenia risk genes (Figure 3a), indicating that the *Der1* mutation and genetic risk factors for schizophrenia converge upon the same pathways.

Enrichment for dysregulation of schizophrenia candidate gene orthologues was also apparent using the heterozygous *Der1* hippocampus combined RNAseq DESeq2 plus DEXSeq data (Table 2, Supplementary Table 2c, d), although there were too few genes to carry out meaningful pathway analysis.

Large-scale genetic data are also available for bipolar disorder and depression[4-6]. IPA did not find that the genes identified from these studies converge strongly upon any canonical pathways, although a subset of depression-associated genes are involved in synaptic structure and activity[6]. Nonetheless, there is enrichment for dysregulation of the orthologues of candidate genes for both disorders in *Der1* cortex, and for depression in *Der1* hippocampus (Table 2, Supplementary Table 2). Moreover, the dysregulated putative depression risk gene orthologues in *Der1* cortex predict effects upon the 'CREB signalling in neurons' pathway (Figure 3a).

We also examined overlaps between genes dysregulated in the *Der1* mouse and two non-psychiatric illness related large-scale GWAS. For Alzheimer's Disease[55] there is enrichment for dysregulation of candidate gene orthologues in *Der1* cortex (Table 2, Supplementary Table 2), with six of the nine gene matches (ABCA7, APOE, CLU, FERMT2, PTK2B/PYK2, SORL1) involved in Amyloid-Beta (Aβ)-related processes[56-61]. This effect may be explained by observations that DISC1 interacts with Amyloid Precursor Protein[62], and regulates Aβ generation[63, 64]. The second comparison was to a study of cerebral cortex architecture[65]. Again, there is enrichment for dysregulation of candidate gene orthologues in *Der1* cortex (Table 2, Supplementary Table 2), although no molecular pathways are highlighted.

The enrichment for dysregulation of orthologues of candidate genes for brain disorders (which is particularly striking for schizophrenia) when combined with convergence upon specific molecular pathways already implicated in those disorders, indicates that the *Der1* mutation may exert effects that are directly relevant to these human brain illnesses.

Discussion

Heterozygous *Der1* mutant mice accurately recapitulate the effects of the t(1:11) translocation upon DISC1 expression in IPSC-derived neural precursors and cortical neurons[12]. We now demonstrate that patterns of gene expression dysregulation and

pathway predictions are similar between heterozygous *Der1* cortex, and IPSC-derived cortical neuronal cultures from t(1:11) translocation carriers. Together these observations suggest that *DISC1* disruption is an important factor in the increased risk of major mental illness displayed by t(1:11) translocation carriers, and argue that the *Der1* mouse model can be used to study the neuronal effects of *DISC1* disruption upon brain function to understand disease mechanisms in these individuals.

Many of the findings reported here are consistent with known DISC1 biology and brain function, but observations such as the lack of overt brain structural changes, and of increased density of hippocampal Parvalbumin-expressing interneurons were unexpected on the basis of previously described DISC1 mutant mice which model aspects of the effects of the t(1;11) translocation upon DISC1 expression[35] (Supplementary Table 8). Such differences, and the many phenotypic differences between previously published mutants (Supplementary Table 8), accentuate the critical importance of studying a mutant that accurately mimics all effects of the t(1;11) translocation in order to understand disease mechanisms in t(1;11) translocation carriers. Other findings, such as the predicted dysregulation of astrocyte lipid metabolism, have not been reported previously. This is the first, and only, mutant mouse to accurately model effects of the t(1:11) translocation, and it therefore provides important and new insights into molecular mechanisms underlying the increased disease risk and psychiatric symptoms of t(1:11) translocation carriers.

Structural and functional brain abnormalities have been reported in human t(1:11) translocation carriers[11], whereas none were detected in the adult *Der1* mice studied here. This difference may reflect fundamental species differences in brain structure and development, and/or secondary genetic or environmental factors consequent upon, or interacting with, the t(1:11) translocation event. Genetic effects may include loss of normal function of the additional disrupted genes *DISC2* and *DISC1FP1*[13, 29], or an influence of genetic modifiers[28]. Environmental effects may include greater relative age, and duration of chronic mental illness with associated long-term exposure to medication such as

antipsychotic drugs. The latter progressively decreases grey matter volume in schizophrenia patients[66], and decreases cortical volume in rats[67].

The absence of brain structural changes, together with the lack of evidence for altered cell class proportions from RNASeq data deconvolution, indicates that the subtle transcriptomic and proteomic alterations identified in the *Der1* mouse are principally due to altered cellular properties that are largely conserved between it and t(1:11) translocation carriers. EWCE analysis of RNASeq data suggests that the *Der1* mutation may target distinct cell types including pyramidal neurons (CA1 and somatosensory) and interneurons. These findings correlate well with a previous EWCE analysis using large-scale schizophrenia GWAS data[2, 34] which found that schizophrenia-associated SNPs map to genomic loci containing genes that are highly expressed in a limited number of brain cell types including CA1 and somatosensory pyramidal neurons, and interneurons[34], thus implicating these cell types in the aetiology of schizophrenia. The additional cell types that appear to be targeted by the *Der1* mutation: dopaminergic neurons, oxytocin/vasopressin-expressing neurons and astrocytes/ependymocytes, were not implicated in schizophrenia by the genomic EWCE analysis. However, dopamine signalling is heavily implicated in schizophrenia, in part because all antipsychotic drugs in clinical use target the dopamine D2 receptor[68], while *DRD2* is located at a genetic locus repeatedly found to associate with schizophrenia[1, 2] and also with depression[6]. The neuropeptides oxytocin and vasopressin regulate many processes, including social behaviour and anxiety[69], and are widely implicated in psychiatric disorders[70]. Astrocyte abnormalities have also been reported in relation to psychiatric disorders[71]. Thus, even if not directly targeted by genomic risk variants, these additional cell types do apparently contribute to psychiatric illness.

Pyramidal neurons are the major excitatory neurons in the brain. Interneurons are inhibitory and regulate neuronal network excitability, primarily of pyramidal neurons. Our analyses suggest widespread targeting of pyramidal neurons and interneurons by the *Der1* mutation, thus excitation and inhibitory control of neuronal networks may be impaired. Neuronal activity could be further impaired if the EWCE predictions are correct and

glutamate uptake by astrocytes is dysregulated. Our findings and predictions relating to pyramidal neurons, which are glutamatergic cells, and to astrocytic glutamate uptake, may be related to the decreased glutamate levels detected by brain imaging of t(1:11) translocation carriers[9]. Altered lipid production by astrocytes may be an additional factor affecting neuronal activity. Lipids are required for many processes, including synaptic activity[47] and myelination[48]. We have previously demonstrated impaired myelination in *Der1* cortex which is presumably due, at least partially, to direct effects of the mutation upon oligodendrocytes because the corresponding IPSC-derived oligodendrocytes from t(1:11) translocation carriers are abnormal[46]. EWCE analysis did not, however, find evidence that oligodendrocytes are strongly targeted by the *Der1* mutation, although some genes highly specific for this cell type are dysregulated, such as Myelin-Oligodendrocyte-Glycoprotein in cortex (Supplementary Table 2a), while genes that impact myelination are dysregulated in hippocampus (Supplementary Table 4b, 5). Altered lipid production by astrocytes could therefore be a contributory factor in the myelination phenotype.

Consistent with the targeting of cell types implicated in schizophrenia, the *Der1* mutation dysregulates orthologues of many genes implicated as risk factors for schizophrenia and depressive disorders through large-scale genome-wide association and CNV studies, as we have previously shown for the t(1:11) translocation in IPSC-derived neurons[12]. The pathways by which the t(1:11) translocation causes major mental illness may therefore overlap those targeted by common genetic risk factors for schizophrenia and depression. We speculate that disruption of the gene encoding the molecular scaffold DISC1, with knock-on effects for its numerous binding partners and functions can, at least partially, recapitulate the consequences of the more common scenario in psychiatric patients whereby multiple interacting common genetic risk factors are inherited, with both scenarios converging upon the same biological pathways. In agreement with this, the symptoms of t(1:11) translocation carriers are indistinguishable from the typical spectrum of clinical presentation of the psychiatric disorders with which they are diagnosed.

The convergence of the *Der1* mutation with a subset of putative common genetic risk factors for schizophrenia and depressive disorders, and the convergence of this subset of genes upon synapses and synaptic plasticity[6, 54] implies that, of all the *Der1* cortex pathway predictions, dysregulated neurotransmission and synaptic plasticity are among the most critical factors in the psychiatric symptoms of t(1:11) translocation carriers. Notably, synaptic plasticity underpins cognition, which is characteristically impaired in schizophrenia.

Altogether, the EWCE and pathway analyses pointing to potential pyramidal neuron and interneuron dysfunction in hippocampus; the evidence that the number of apoptotic cells in CA1 may be increased; the higher density of hippocampal Parvalbumin-positive interneurons; the extensive changes to synaptic protein expression in hippocampus synaptosomes; and the electrophysiology data indicating reduced AMPA:NMDA ratio in cultured hippocampal neurons, suggest that hippocampal circuits are especially sensitive to the mutation, although effects upon other brain regions are also likely.

The hippocampus has multiple input/output pathways from/to other brain regions which are regulated by various neurotransmitters. Hippocampal dysfunction in *Der1* mice could thus have numerous extrinsic/intrinsic causes, and knock-on effects. CA1 pyramidal neurons provide the major hippocampal output, including the hippocampal-to-PFC pathway that regulates NMDA receptor-dependent LTP and cognition[72]. This pathway is widely implicated in psychiatric disorders[72]. It is thus an exemplar of the mechanisms by which *DISC1* disruption could confer susceptibility to major mental illness by bringing together the diverse effects described here, and elsewhere[12, 46], in our studies of neural cells derived from t(1:11) translocation carriers, and of the corresponding *Der1* mouse. Our findings thus provide important insights into potential disease mechanisms involving specific molecular pathways/functions and cell types in t(1:11) translocation carriers that are likely relevant to schizophrenia and affective disorders in general.

Acknowledgements

We thank the t(1:11) translocation family members who have taken part in our research by donating skin biopsies for reprogramming and production of neural cells. This work was funded by MRC grant MR/J004367/1; Brain & Behavior Research Foundation Independent Investigator Grant 23306 and Young Investigator Grant 27404; European Union Seventh Framework Programme 607616FP7, Deciphering inter- and intracellular signalling in schizophrenia; a bequest from Eva Lester; Scottish Funding Council Scottish Senior Fellowship and Chief Scientists Office Senior Clinical fellowship Starter Grant awards to AMM; the University of Edinburgh Wellcome Trust Institutional Support Fund grant J22734, a Sir Henry Wellcome postdoctoral fellowship (213674/Z/18/Z) awarded to DMH; EUREKA/European Union Eurostars E! 7675; and an NWO Gravitation project: A Roadmap from Neurogenetics to Neurobiology (NWO: 024.004.0212).

Conflict of interest statement

The authors declare no competing financial interests. AMM has received research support from Eli Lilly and Company, Janssen and the Sackler Trust, and speaker fees from Illumina and Janssen. ACV has received research support from F. Hoffman La Roche and UCB Biopharma SPRL. ML is a full time employee of Sylics (Synaptologics B.V.), a private company that offers mouse phenotyping services. ABS is shareholder of Alea Biotech B.V., a holding of Sylics (Synaptologics B.V.). MD is based at Sanofi.

559 **Table 1** Top relevant altered cellular functions in heterozygous *Der1* mouse cortex and
560 human IPSC-derived neurons from members of the t(1:11) translocation family predicted
561 using DESeq2+DEXSeq data. All *Der1* mouse and human t(1;11) neuron functions are listed
562 in Supplementary Table 4.

Function (no. of molecules[a])	***Der1* cortex score (no. of genes[b])**	**Human t(1:11) translocation neuron culture score (no. of genes[b])**	**Hypergeometric p value for enrichment (no. of shared genes[c])**
General cell morphology			
Development of neurons (1,423)	p=2e-53 (457)	p=2e-13 (148)	**p=1e-3** (63)
Morphogenesis of neurons (1,080)	p=1e-47 (360)	p=4e-13 (119)	**p=3e-4** (56)
Morphology of neurons (1,123)	p=7e-37 (303)	p=1e-4 (80)	**p=6e-5** (37)
Morphology of cells (4,370)	p=1e-29 (902)		
Abnormal morphology of neurons (923)	p=6e-25 (212)		
Cell contact			
Cell-cell contact (1,118)	p=5e-26 (299)	p=4e-6 (92)	**p=6e-4** (38)
Development of gap junctions (327)	p=1e-18 (123)	p=2e-4 (37)	*p=0.08* (17)
Formation of cell-cell contacts (414)	p=6e-16 (138)	p=8e-6 (48)	*p=0.08* (19)
Formation of intercellular junctions (409)	p=1e-15 (136)	p=1e-5 (47)	*p=0.07* (19)
Formation of plasma membrane (406)	p=1e-15 (134)	p=3e-6 (48)	*p=0.05* (20)
Cytoskeleton			
Organization of cytoplasm (2,832)	p=2e-64 (791)	p=3e-16 (257)	**p=2e-6** (104)
Organization of cytoskeleton (2,624)	p=4e-57 (720)	p=3e-16 (240)	**p=1e-8** (101)
Microtubule dynamics (2,247)	p=6e-54 (627)	p=1e-14 (206)	**p=1e-6** (87)
Development of cytoplasm (873)	p=9e-19 (233)	p=2e-4 (71)	**p=1e-5** (35)
Formation of cytoskeleton (733)	p=5e-14 (179)		
Cellular protrusions/neurites			
Neuritogenesis (1,067)	p=2e-46 (354)	p=4e-12 (115)	**p=2e-4** (55)
Formation of cellular protrusions (1,645)	p=1e-46 (488)	p=3e-15 (170)	**p=2e-4** (70)
Growth of neurites (910)	p=5e-30 (261)	p=1e-7 (81)	**p=6e-4** (36)
Morphology of cellular protrusions (522)	p=3e-25 (166)		
Morphology of neurites (414)	p=6e-25 (139)		
Axons			
Axonogenesis (338)	p=1e-18 (122)	p=2e-7 (45)	**p=2e-3** (25)
Morphology of axons (169)	p=2e-16 (65)		
Growth of axons (281)	p=2e-12 (87)		
Abnormal morphology of axons (133)	p=4e-11 (46)		
Guidance of axons (202)	p=5e-10 (71)	p=2e-5 (29)	ns (12)
Dendrites			
Formation of dendrites (209)	p=9e-19 (90)		
Dendritic growth/branching (446)	p=8e-18 (131)		
Density of dendritic spines (143)	p=1e-11 (49)		
Morphology of dendrites (138)	p=3e-9 (49)		
Abnormal morphology of dendrites (75)	p=3e-8 (32)		
Cell proliferation			
Proliferation of neuronal cells (1066)	p=5e-28 (290)	p=2e-9 (98)	**p=2e-3** (39)
Neuronal migration			
Migration of neurons (362)	p=1e-16 (125)	p=8e-6 (43)	**p=0.03** (20)
Circadian rhythm			
Circadian rhythm (132)	p=3e-8 (55)		
Transport			
Organisation of organelle (948)	p=1e-23 (270)		
Transport of vesicles (192)	p=1e-14 (69)		
Endocytosis (924)	p=8e-10 (202)	p=3e-6 (76)	**p=2e-3** (27)
Secretory pathway (367)	p=8e-10 (93)		
Formation of vesicles (307)	p=4e-9 (70)		
Neurotransmission			
Neurotransmission (716)	p=5e-31 (233)	p=5e-5 (62)	**p=0.03** (26)
Potentiation of synapse (546)	p=1e-28 (165)		
Long-term potentiation (539)	p=4e-28 (163)		
Synaptic transmission (558)	p=4e-27 (191)	p=7e-06 (55)	**p=0.04** (24)
Developmental process of synapse (303)	p=2e-18 (117)	p=1e-4 (36)	*p=0.08* (17)
Excitatory postsynaptic potential (166)	p=2e-15 (72)		
Long-term potentiation of brain (281)	p=2e-13 (74)		
Plasticity of synapse (170)	p=2e-12 (66)		

Long-term potentiation of cerebral cortex (254)	p=6e-12 (66)		
Miniature excitatory postsynaptic currents (71)	p=1e-11 (38)		

A full list of functions is provided in Supplementary Table 4a, d. Related functions are grouped, with top functions shown for each group. a, total number of molecules relating to each IPA function; b, number of dysregulated genes relating to each function; c, number of genes relating to function that are dysregulated in both *Der1* cortex and human t(1:11) translocation neurons; italics, trend; ns, not significant

570 **Table 2** Enrichment for dysregulated expression of putative psychiatric illness risk gene

571 orthologues in *Der1* cortex and hippocampus.

Study	Loci	Genes	Dysregulated in cortex	Hypergeometric p value for enrichment in cortex	Dysregulated in hippocampus	Hypergeometric p value for enrichment in hippocampus
GWAS, schizophrenia[1]	108	348	121 genes at 61 loci	**p=1e-13** (**p=8e-19**)	6 genes at 6 loci	**p=0.04** (**p=2e-4**)
GWAS, schizophrenia[2]	143	481	127 genes at 73 loci	**p=3e-6** (**p=8e-19**)	6 genes at 6 loci	*p=0.09* (**p=8e-4**)
MAGMA, schizophrenia[2]		535	210	**p=3e-30**	15	**p=2e-5**
CNV (synapse genes), schizophrenia[3]		52	25	**p=8e-7**	4	**p=7e-4**
GWAS, depression[4]	44	70	19 at 19 loci	**p=0.02** (**p=9e-5**)	1	ns
MAGMA, depression[4]		153	33	**p=0.047**	1	ns
MAGMA meta-analysis, depression[6]		269	94	**p=4e-11**	6	**p=0.01**
GWAS, bipolar disorder[5]	30	218	73 at 21 loci	**p=4e-8** (**p=8e-10**)	3 genes at 3 loci	ns (**p=2e-3**)
MAGMA, bipolar disorder[5]		152	49	**p=2e-5**	3	*p=0.09*
GWAS, Alzheimer's Disease[55]	21	102	9 at 9 loci	**p=3e-3 (p=6e-3)**	1	ns
GWAS cerebral cortex architecture[65]		193	57	**p=5e-5**	1	ns

572

573 Loci indicates the number of associated genomic loci identified by GWAS. Genes indicates

574 the total number of genes at the associated loci, or the total number identified by MAGMA.

575 Bracketed p values indicate enrichment for loci containing at least one dysregulated gene

576 orthologue. italics, trend; ns, not significant

577

References

1. Schizophrenia Working Group of the Psychiatric Genomics C. Biological insights from 108 schizophrenia-associated genetic loci. *Nature* 2014; **511**(7510)**:** 421-427.

2. Pardinas AF, Holmans P, Pocklington AJ, Escott-Price V, Ripke S, Carrera N *et al.* Common schizophrenia alleles are enriched in mutation-intolerant genes and in regions under strong background selection. *Nature genetics* 2018; **50**(3)**:** 381-389.

3. Cnv, Schizophrenia Working Groups of the Psychiatric Genomics C, Psychosis Endophenotypes International C. Contribution of copy number variants to schizophrenia from a genome-wide study of 41,321 subjects. *Nature genetics* 2017; **49**(1)**:** 27-35.

4. Wray NR, Ripke S, Mattheisen M, Trzaskowski M, Byrne EM, Abdellaoui A *et al.* Genome-wide association analyses identify 44 risk variants and refine the genetic architecture of major depression. *Nature genetics* 2018; **50**(5)**:** 668-681.

5. Stahl EA, Breen G, Forstner AJ, McQuillin A, Ripke S, Trubetskoy V *et al.* Genome-wide association study identifies 30 loci associated with bipolar disorder. *Nature genetics* 2019; **51**(5)**:** 793-803.

6. Howard DM, Adams MJ, Clarke TK, Hafferty JD, Gibson J, Shirali M *et al.* Genome-wide meta-analysis of depression identifies 102 independent variants and highlights the importance of the prefrontal brain regions. *Nature neuroscience* 2019; **22**(3)**:** 343-352.

7. St Clair D, Blackwood D, Muir W, Carothers A, Walker M, Spowart G *et al.* Association within a family of a balanced autosomal translocation with major mental illness. *Lancet* 1990; **336**(8706)**:** 13-16.

8. Blackwood DH, Fordyce A, Walker MT, St Clair DM, Porteous DJ, Muir WJ. Schizophrenia and affective disorders--cosegregation with a translocation at chromosome 1q42 that directly disrupts brain-expressed genes: clinical and P300 findings in a family. *American journal of human genetics* 2001; **69**(2)**:** 428-433.

9. Thomson PA, Duff B, Blackwood DH, Romaniuk L, Watson A, Whalley HC *et al.* Balanced translocation linked to psychiatric disorder, glutamate, and cortical structure/function. *NPJ Schizophr* 2016; **2:** 16024.

10. Whalley HC, Dimitrova R, Sprooten E, Dauvermann MR, Romaniuk L, Duff B *et al.* Effects of a Balanced Translocation between Chromosomes 1 and 11 Disrupting the DISC1 Locus on White Matter Integrity. *PLoS One* 2015; **10**(6)**:** e0130900.

11. Doyle OM, Bois C, Thomson P, Romaniuk L, Whitcher B, Williams SC *et al.* The cortical thickness phenotype of individuals with DISC1 translocation resembles schizophrenia. *J Clin Invest* 2015; **125**(9)**:** 3714-3722.

12. Malavasi ELV, Economides KD, Grunewald E, Makedonopoulou P, Gautier P, Mackie S *et al.* DISC1 regulates N-methyl-D-aspartate receptor dynamics: abnormalities induced by a Disc1 mutation modelling a translocation linked to major mental illness. *Transl Psychiatry* 2018; **8**(1)**:** 184.

13. Millar JK, Wilson-Annan JC, Anderson S, Christie S, Taylor MS, Semple CA *et al.* Disruption of two novel genes by a translocation co-segregating with schizophrenia. *Human molecular genetics* 2000; **9**(9)**:** 1415-1423.

14. Camargo LM, Collura V, Rain JC, Mizuguchi K, Hermjakob H, Kerrien S *et al.* Disrupted in Schizophrenia 1 Interactome: evidence for the close connectivity of risk genes and a potential synaptic basis for schizophrenia. *Molecular psychiatry* 2007; **12**(1)**:** 74-86.

15. Brandon NJ, Millar JK, Korth C, Sive H, Singh KK, Sawa A. Understanding the role of DISC1 in psychiatric disease and during normal development. *J Neurosci* 2009; **29**(41)**:** 12768-12775.

16. Mao Y, Ge X, Frank CL, Madison JM, Koehler AN, Doud MK *et al.* Disrupted in schizophrenia 1 regulates neuronal progenitor proliferation via modulation of GSK3beta/beta-catenin signaling. *Cell* 2009; **136**(6)**:** 1017-1031.

17. Duan X, Chang JH, Ge S, Faulkner RL, Kim JY, Kitabatake Y *et al.* Disrupted-In-Schizophrenia 1 regulates integration of newly generated neurons in the adult brain. *Cell* 2007; **130**(6)**:** 1146-1158.

18. Kamiya A, Kubo K, Tomoda T, Takaki M, Youn R, Ozeki Y *et al.* A schizophrenia-associated mutation of DISC1 perturbs cerebral cortex development. *Nature cell biology* 2005; **7**(12)**:** 1167-1178.

19. Ogawa F, Malavasi EL, Crummie DK, Eykelenboom JE, Soares DC, Mackie S *et al.* DISC1 complexes with TRAK1 and Miro1 to modulate anterograde axonal mitochondrial trafficking. *Human molecular genetics* 2014; **23**(4)**:** 906-919.

20. Atkin TA, MacAskill AF, Brandon NJ, Kittler JT. Disrupted in Schizophrenia-1 regulates intracellular trafficking of mitochondria in neurons. *Molecular psychiatry* 2011; **16**(2)**:** 122-124, 121.

21. Flores R, 3rd, Hirota Y, Armstrong B, Sawa A, Tomoda T. DISC1 regulates synaptic vesicle transport via a lithium-sensitive pathway. *Neurosci Res* 2011; **71**(1)**:** 71-77.

22. Tsuboi D, Kuroda K, Tanaka M, Namba T, Iizuka Y, Taya S *et al.* Disrupted-in-schizophrenia 1 regulates transport of ITPR1 mRNA for synaptic plasticity. *Nature neuroscience* 2015; **18**(5)**:** 698-707.

23. Wei J, Graziane NM, Gu Z, Yan Z. DISC1 Protein Regulates gamma-Aminobutyric Acid, Type A (GABAA) Receptor Trafficking and Inhibitory Synaptic Transmission in Cortical Neurons. *The Journal of biological chemistry* 2015; **290**(46)**:** 27680-27687.

24. Wei J, Graziane NM, Wang H, Zhong P, Wang Q, Liu W *et al.* Regulation of N-Methyl-D-Aspartate Receptors by Disrupted-in-Schizophrenia-1. *Biological psychiatry* 2013.

25. Wen Z, Nguyen HN, Guo Z, Lalli MA, Wang X, Su Y *et al.* Synaptic dysregulation in a human iPS cell model of mental disorders. *Nature* 2014.

26. Tropea D, Molinos I, Petit E, Bellini S, Nagakura I, O'Tuathaigh C *et al.* Disrupted in schizophrenia 1 (DISC1) L100P mutants have impaired activity-dependent plasticity in vivo and in vitro. *Transl Psychiatry* 2016; **6:** e712.

27. Zhou X, Geyer MA, Kelsoe JR. Does disrupted-in-schizophrenia (DISC1) generate fusion transcripts? *Molecular psychiatry* 2008; **13**(4)**:** 361-363.

28. Ryan NM, Lihm J, Kramer M, McCarthy S, Morris SW, Arnau-Soler A *et al.* DNA sequence-level analyses reveal potential phenotypic modifiers in a large family with psychiatric disorders. *Molecular psychiatry* 2018.

29. Eykelenboom JE, Briggs GJ, Bradshaw NJ, Soares DC, Ogawa F, Christie S *et al.* A t(1;11) translocation linked to schizophrenia and affective disorders gives rise to aberrant chimeric DISC1 transcripts that encode structurally altered, deleterious mitochondrial proteins. *Human molecular genetics* 2012; **21**(15)**:** 3374-3386.

30. Tropea D, Hardingham N, Millar K, Fox K. Mechanisms underlying the role of DISC1 in synaptic plasticity. *The Journal of physiology* 2018; **596**(14)**:** 2747-2771.

31. Love MI, Huber W, Anders S. Moderated estimation of fold change and dispersion for RNA-seq data with DESeq2. *Genome biology* 2014; **15**(12)**:** 550.

32. Anders S, Reyes A, Huber W. Detecting differential usage of exons from RNA-seq data. *Genome Res* 2012; **22**(10)**:** 2008-2017.

33. Skene NG, Grant SG. Identification of Vulnerable Cell Types in Major Brain Disorders Using Single Cell Transcriptomes and Expression Weighted Cell Type Enrichment. *Front Neurosci* 2016; **10:** 16.

34. Skene NG, Bryois J, Bakken TE, Breen G, Crowley JJ, Gaspar HA *et al.* Genetic identification of brain cell types underlying schizophrenia. *Nature genetics* 2018; **50**(6)**:** 825-833.

35. Brandon NJ, Sawa A. Linking neurodevelopmental and synaptic theories of mental illness through DISC1. *Nature reviews* 2011; **12**(12)**:** 707-722.

36. Newman AM, Liu CL, Green MR, Gentles AJ, Feng W, Xu Y *et al.* Robust enumeration of cell subsets from tissue expression profiles. *Nat Methods* 2015; **12**(5)**:** 453-457.

37. Park YU, Jeong J, Lee H, Mun JY, Kim JH, Lee JS *et al.* Disrupted-in-schizophrenia 1 (DISC1) plays essential roles in mitochondria in collaboration with Mitofilin. *Proceedings of the National Academy of Sciences of the United States of America* 2010; **107**(41)**:** 17785-17790.

38. Pinero-Martos E, Ortega-Vila B, Pol-Fuster J, Cisneros-Barroso E, Ruiz-Guerra L, Medina-Dols A *et al.* Disrupted in schizophrenia 1 (DISC1) is a constituent of the mammalian mitochondrial contact site and cristae organizing system (MICOS) complex, and is essential for oxidative phosphorylation. *Human molecular genetics* 2016.

39. Wang Q, Charych EI, Pulito VL, Lee JB, Graziane NM, Crozier RA *et al.* The psychiatric disease risk factors DISC1 and TNIK interact to regulate synapse composition and function. *Molecular psychiatry* 2011; **16**(10)**:** 1006-1023.

40. Jaaro-Peled H, Altimus C, LeGates T, Cash-Padgett T, Zoubovsky S, Hikida T *et al.* Abnormal wake/sleep pattern in a novel gain-of-function model of DISC1. *Neurosci Res* 2016; **112:** 63-69.

41. Seshadri S, Faust T, Ishizuka K, Delevich K, Chung Y, Kim SH *et al.* Interneuronal DISC1 regulates NRG1-ErbB4 signalling and excitatory-inhibitory synapse formation in the mature cortex. *Nat Commun* 2015; **6:** 10118.

42. Tang W, Thevathasan JV, Lin Q, Lim KB, Kuroda K, Kaibuchi K *et al.* Stimulation of Synaptic Vesicle Exocytosis by the Mental Disease Gene DISC1 is Mediated by N-Type Voltage-Gated Calcium Channels. *Front Synaptic Neurosci* 2016; **8:** 15.

43. Hattori T, Shimizu S, Koyama Y, Yamada K, Kuwahara R, Kumamoto N *et al.* DISC1 regulates cell-cell adhesion, cell-matrix adhesion and neurite outgrowth. *Molecular psychiatry* 2010; **15**(8)**:** 778, 798-809.

44. Shimizu S, Koyama Y, Hattori T, Tachibana T, Yoshimi T, Emoto H *et al.* DBZ, a CNS-specific DISC1 binding protein, positively regulates oligodendrocyte differentiation. *Glia* 2014; **62**(5)**:** 709-724.

45. Hattori T, Shimizu S, Koyama Y, Emoto H, Matsumoto Y, Kumamoto N *et al.* DISC1 (disrupted-in-schizophrenia-1) regulates differentiation of oligodendrocytes. *PLoS One* 2014; **9**(2)**:** e88506.

46. Vasistha NA, Johnstone M, Barton SK, Mayerl SE, Thangaraj Selvaraj B, Thomson PA *et al.* Familial t(1;11) translocation is associated with disruption of white matter structural integrity and oligodendrocyte-myelin dysfunction. *Molecular psychiatry* 2019.

47. van Deijk AF, Camargo N, Timmerman J, Heistek T, Brouwers JF, Mogavero F *et al.* Astrocyte lipid metabolism is critical for synapse development and function in vivo. *Glia* 2017; **65**(4)**:** 670-682.

48. Camargo N, Goudriaan A, van Deijk AF, Otte WM, Brouwers JF, Lodder H *et al.* Oligodendroglial myelination requires astrocyte-derived lipids. *PLoS Biol* 2017; **15**(5)**:** e1002605.

49. Mahan VL. Neurointegrity and neurophysiology: astrocyte, glutamate, and carbon monoxide interactions. *Med Gas Res* 2019; **9**(1)**:** 24-45.

50. Prytkova I, Brennand KJ. Prospects for Modeling Abnormal Neuronal Function in Schizophrenia Using Human Induced Pluripotent Stem Cells. *Front Cell Neurosci* 2017; **11:** 360.

51. Koopmans F, van Nierop P, Andres-Alonso M, Byrnes A, Cijsouw T, Coba MP *et al.* SynGO: An Evidence-Based, Expert-Curated Knowledge Base for the Synapse. *Neuron* 2019; **103**(2)**:** 217-234 e214.

52. Chen SY, Huang PH, Cheng HJ. Disrupted-in-Schizophrenia 1-mediated axon guidance involves TRIO-RAC-PAK small GTPase pathway signaling. *Proceedings of the National Academy of Sciences of the United States of America* 2011; **108**(14)**:** 5861-5866.

53. Ba W, Yan Y, Reijnders MR, Schuurs-Hoeijmakers JH, Feenstra I, Bongers EM *et al.* TRIO loss of function is associated with mild intellectual disability and affects dendritic branching and synapse function. *Human molecular genetics* 2016; **25**(5)**:** 892-902.

54. Hall J, Trent S, Thomas KL, O'Donovan MC, Owen MJ. Genetic risk for schizophrenia: convergence on synaptic pathways involved in plasticity. *Biological psychiatry* 2015; **77**(1)**:** 52-58.

55. Kunkle BW, Grenier-Boley B, Sims R, Bis JC, Damotte V, Naj AC *et al.* Genetic meta-analysis of diagnosed Alzheimer's disease identifies new risk loci and implicates Abeta, tau, immunity and lipid processing. *Nature genetics* 2019; **51**(3)**:** 414-430.

56. Sakae N, Liu CC, Shinohara M, Frisch-Daiello J, Ma L, Yamazaki Y *et al.* ABCA7 Deficiency Accelerates Amyloid-beta Generation and Alzheimer's Neuronal Pathology. *J Neurosci* 2016; **36**(13)**:** 3848-3859.

57. Holtzman DM. Role of apoe/Abeta interactions in the pathogenesis of Alzheimer's disease and cerebral amyloid angiopathy. *J Mol Neurosci* 2001; **17**(2)**:** 147-155.

58. Li X, Ma Y, Wei X, Li Y, Wu H, Zhuang J *et al.* Clusterin in Alzheimer's disease: a player in the biological behavior of amyloid-beta. *Neurosci Bull* 2014; **30**(1)**:** 162-168.

59. Chapuis J, Flaig A, Grenier-Boley B, Eysert F, Pottiez V, Deloison G *et al.* Genome-wide, high-content siRNA screening identifies the Alzheimer's genetic risk factor FERMT2 as a major modulator of APP metabolism. *Acta neuropathologica* 2017; **133**(6)**:** 955-966.

60. Salazar SV, Cox TO, Lee S, Brody AH, Chyung AS, Haas LT *et al.* Alzheimer's Disease Risk Factor Pyk2 Mediates Amyloid-beta-Induced Synaptic Dysfunction and Loss. *J Neurosci* 2019; **39**(4)**:** 758-772.

61. Alexopoulos P, Kurz A, Lewczuk P, Kornhuber J, Wiltfang J, Maier W *et al.* The sortilin-related receptor SORL1 and the amyloid cascade: a possible explanation for the concurrent elevation of CSF soluble APPalpha and APPbeta in Alzheimer's disease. *Int J Geriatr Psychiatry* 2010; **25**(5)**:** 542-543.

62. Young-Pearse TL, Suth S, Luth ES, Sawa A, Selkoe DJ. Biochemical and functional interaction of disrupted-in-schizophrenia 1 and amyloid precursor protein regulates neuronal migration during mammalian cortical development. *J Neurosci* 2010; **30**(31)**:** 10431-10440.

831 63. Shahani N, Seshadri S, Jaaro-Peled H, Ishizuka K, Hirota-Tsuyada Y, Wang Q *et al.*
832 DISC1 regulates trafficking and processing of APP and Abeta generation. *Molecular*
833 *psychiatry* 2015; **20**(7)**:** 874-879.

834

835 64. Deng QS, Dong XY, Wu H, Wang W, Wang ZT, Zhu JW *et al.* Disrupted-in-
836 Schizophrenia-1 Attenuates Amyloid-beta Generation and Cognitive Deficits in
837 APP/PS1 Transgenic Mice by Reduction of beta-Site APP-Cleaving Enzyme 1
838 Levels. *Neuropsychopharmacology* 2016; **41**(2)**:** 440-453.

839

840 65. Grasby KL, Jahanshad N, Painter JN, Colodro-Conde L, Bralten J, Hibar DP *et al.*
841 The genetic architecture of the human cerebral cortex. *Science (New York, NY* 2020;
842 **367**(6484).

843

844 66. Fusar-Poli P, Smieskova R, Kempton MJ, Ho BC, Andreasen NC, Borgwardt S.
845 Progressive brain changes in schizophrenia related to antipsychotic treatment? A
846 meta-analysis of longitudinal MRI studies. *Neurosci Biobehav Rev* 2013; **37**(8)**:** 1680-
847 1691.

848

849 67. Vernon AC, Crum WR, Lerch JP, Chege W, Natesan S, Modo M *et al.* Reduced
850 cortical volume and elevated astrocyte density in rats chronically treated with
851 antipsychotic drugs-linking magnetic resonance imaging findings to cellular
852 pathology. *Biological psychiatry* 2014; **75**(12)**:** 982-990.

853

854 68. Sonnenschein SF, Grace AA. Insights on current and novel antipsychotic
855 mechanisms from the MAM model of schizophrenia. *Neuropharmacology* 2019.

856

69. Bredewold R, Veenema AH. Sex differences in the regulation of social and anxiety-related behaviors: insights from vasopressin and oxytocin brain systems. *Curr Opin Neurobiol* 2018; **49:** 132-140.

70. Iovino M, Messana T, De Pergola G, Iovino E, Dicuonzo F, Guastamacchia E *et al.* The Role of Neurohypophyseal Hormones Vasopressin and Oxytocin in Neuropsychiatric Disorders. *Endocr Metab Immune Disord Drug Targets* 2018; **18**(4)**:** 341-347.

71. Elsayed M, Magistretti PJ. A New Outlook on Mental Illnesses: Glial Involvement Beyond the Glue. *Front Cell Neurosci* 2015; **9:** 468.

72. Godsil BP, Kiss JP, Spedding M, Jay TM. The hippocampal-prefrontal pathway: the weak link in psychiatric disorders? *Eur Neuropsychopharmacol* 2013; **23**(10)**:** 1165-1181.

73. Pandya NJ, Koopmans F, Slotman JA, Paliukhovich I, Houtsmuller AB, Smit AB *et al.* Correlation profiling of brain sub-cellular proteomes reveals co-assembly of synaptic proteins and subcellular distribution. *Sci Rep* 2017; **7**(1)**:** 12107.

877 **Legends to figures**

878 **Fig. 1** The *Der1* mutation targets specific cell types in heterozygous cortex and
879 hippocampus. **a** *Disc1* RNASeq reads normalised to total reads per sample in wild-type
880 versus heterozygous *Der1* cortex and hippocampus. **b** Heat maps of the top 500
881 dysregulated genes identified by RNASeq of wild-type versus heterozygous *Der1* cortex and
882 hippocampus. **c d** EWCE analysis of heterozygous *Der1* cortex and hippocampus,
883 respectively, in mouse brain cell classes. asterisk, significance after Bonferroni correction;
884 Emb, embryonic; Hyp, hypothalamic; SD, standard deviation **e** Parvalbumin expression in
885 hippocampal sections from nine week old mouse brain. Enlarged regions showing
886 Parvalbumin-expressing interneurons are indicated by boxes. scale bars, 100μm **f** Average
887 density of Parvalbumin-expressing interneurons. Hippocampus refers to the whole
888 hippocampal formation. Data were analysed by Kruskal-Wallis one-way ANOVA, p=0.07 for
889 the dentate gyrus; p=0.049 for the hippocampal formation. Horizontal line on graphs for each
890 sample, average of values; WT, wild-type; HET, heterozygous *Der1*; HOM, homozygous
891 *Der1*; DG, dentate gyrus; *, p<0.05
892
893 **Fig. 2** Consequences of the *Der1* mutation. **a** Top relevant canonical pathway predictions for
894 heterozygous *Der1* cortex using whole gene, DESeq2, or whole gene and exon level,
895 DESeq2+DEXSeq data. Asterisks indicate pathways highlighted in both cases. Where IPA
896 predicts a direction of change this is indicated by a z score, with positive z scores indicating
897 upregulation. **b** Altered gene expression in the 'CREB signalling in neurons' canonical
898 pathway in heterozygous *Der1* cortex, determined using whole gene and exon level
899 DESeq2+DEXSeq data. To provide additional information, genes encoding calcium channels
900 (CaCh), metabotropic glutamate receptors (mGLUR), ionotropic glutamate receptor subunits
901 (iGLUR) and structural synaptic components have been added to the pathway using the IPA
902 'Build' tool. Transcripts encoding components from the whole pathway are dysregulated at
903 the whole gene and/or isoform level, including ionotropic AMPA and NMDA glutamate
904 receptor subunits, metabotropic glutamate receptors and voltage-gated calcium channels, all

of which can control the calcium ion influx or G-protein activation that initiates the pathway. Genes encoding several synaptic scaffolds that are required to generate and maintain synapse structure/size and/or anchor glutamate receptors and calcium channels are also dysregulated, including Shank1, Homer1 and Dlg1/3/4, neurexins and neuroligins. Also dysregulated are genes encoding various factors downstream of glutamate receptors and calcium channels that activate the cAMP-dependent transcription factor CREB, such as various forms of Camk2, and adenylyl cyclases. The transcriptional machinery is additionally affected, including the cAMP-dependent transcription factor complex. Double outlines indicate protein complexes and classes, the components of which can be found in Supplementary Table 2a, b. Colour intensity represents strength of gene expression change, with graded colour within double outlined symbols representing overall direction of change within protein complexes. green, downregulated; red, upregulated; *genes identified by DEXSeq; ** genes identified by DEXSeq and DESeq2 **c** Sunburst plots showing SynGO annotated synaptic functions of the dysregulated proteins found in homozygous *Der1* hippocampus synaptosomes (FDR adjusted p-value < 0.05). Note that synaptosomes are enriched for the complete presynaptic terminal, the postsynaptic membrane and the postsynaptic density, as well as membranes originating from organelles such as the Golgi and endoplasmic reticulum[73]. **d** Quantification of AMPA and NMDA receptor currents by whole-cell patch clamping of neurons cultured from *Der1* hippocampus. Data were analysed by one-way ANOVA, p=0.03. Horizontal line on graphs for each sample, average of values; WT, wild-type; HET, heterozygous *Der1*; HOM, homozygous *Der1*; *, p<0.05

Fig. 3 The *Der1* mutation dysregulates canonical pathways and genes related to schizophrenia and depression in heterozygous *Der1* cortex. **a** Canonical pathway predictions for putative schizophrenia risk genes, and for orthologues of putative schizophrenia and depression risk genes that are dysregulated at the whole gene and exon level, as identified using DESeq2+DEXSeq data. **b, c** Altered schizophrenia risk gene orthologue expression in the ‘Synaptic long-term depression’ and ‘CREB signalling in neurons’ canonical pathways,

933 respectively. Double outlines indicate protein complexes and classes, the components of
934 which can be found in Supplementary Table 2a, b. To provide additional information, genes
935 encoding ionotropic glutamate receptor δ subunits (Grid), AMPA receptor subunits (AMPAR),
936 voltage-gated calcium channel subunits (VGCC), calcium channels (CaCh), ionotropic
937 glutamate receptor subunits (iGLUR) and structural synaptic components have been added
938 to the pathways using the IPA 'Build' tool. *genes identified by DEXSeq; red, dysregulated
939 putative schizophrenia risk gene orthologue

940

Functional brain defects in a mouse model of a chromosomal t(1;11) translocation that disrupts *DISC1* and confers increased risk of psychiatric illness

Supplementary information

Marion Bonneau[1], Shane T. O'Sullivan[1], Miguel A. Gonzalez-Lozano[2], Paul Baxter[3], Phillippe Gautier[4], Elena Marchisella[5], Neil R. Hardingham[6], Robert A. Chesters[7], Helen Torrance[1], David M. Howard[8, 9], Maurits A. Jansen[10], Melanie McMillan[11], Yasmin Singh[12], Michel Didier[13], Frank Koopmans[2], Colin A. Semple[4], Andrew M. McIntosh[9], Hansjürgen Volkmer[14], Maarten Loos[5], Kevin Fox[6], Giles E. Hardingham[3], Anthony C. Vernon[7, 15], David J. Porteous[1], August B. Smit[2], David J. Price[3], J. Kirsty Millar[1]*

[1]Centre for Genomic and Experimental Medicine, MRC Institute of Genetics and Molecular Medicine at the University of Edinburgh, Edinburgh, UK

[2]Department of Molecular and Cellular Neurobiology, Center for Neurogenomics and Cognitive Research, VU University, Amsterdam, The Netherlands

[3]Centre for Discovery Brain Sciences, Hugh Robson Building, The University of Edinburgh, Edinburgh, UK

[4]MRC Human Genetics Unit, MRC Institute of Genetics and Molecular Medicine at the University of Edinburgh, Edinburgh, UK

[5]Sylics Synaptologics BV, Amsterdam, The Netherlands

[6]School of Biosciences, Museum Avenue, Cardiff University, Cardiff, UK

[7]Department of Basic and Clinical Neuroscience, Institute of Psychiatry, Psychology and Neuroscience, King's College London, London, UK

[8]Social, Genetic and Developmental Psychiatry Centre, Institute of Psychiatry, Psychology & Neuroscience, King's College London, UK

[9]Division of Psychiatry, Kennedy Tower, The University of Edinburgh, Edinburgh, UK

[10]Edinburgh Preclinical Imaging, The Chancellor's Building, The University of Edinburgh, Edinburgh, UK,

[11]Centre for Reproductive Health, The Queen's Medical Research Institute, The University of Edinburgh, Edinburgh, UK

[12]Centre for Genomics and Transcriptomics, Paul-Ehrlich-Straße 23, D-72076, Tübingen, Germany

[13]Translational Sciences at Sanofi, Chilly-Mazarin, France

[14]Department of Molecular Biology, NMI Natural and Medical Sciences Institute at the University of Tübingen, Reutlingen, Germany

[15]MRC Centre for Neurodevelopmental Disorders, King's College London, London, UK

*Corresponding author

Tel: +44 (0)131 651 8732

Fax: +44 (0)131 651 1059

Email: kirsty.millar@igmm.ed.ac.uk

Address: Centre for Genomic and Experimental Medicine, MRC Institute of Genetics and Molecular Medicine at the University of Edinburgh, Crewe Road, Edinburgh, EH4 2XU, UK

Materials and methods

Mouse colony maintenance

Mice were housed in the Biomedical Research Facility at the University of Edinburgh. All mice were maintained in accordance with Home Office regulations, and all protocols were approved by the local ethics committee of the University of Edinburgh. Mouse genotyping was carried out as previously described[1].

Perfusion fixation and brain isolation

Mice were anaesthetized with intraperitoneal injection of 0.1ml/10g Fentanyl/Fluanisone (Hypnorm®) and Midazolam (Hyponovel®). Deep anaesthesia was ensured by measuring withdrawal reflexes. The mice were then transcardially perfused with 4% paraformaldehyde at a rate of 0.2-0.5 ml/second. Brains were dissected out and the olfactory bulbs and cerebellum removed. Brains were transferred to 4% neutral buffered formalin for 24 hr, then stored in 70% ethanol.

Magnetic resonance imaging

Brains were taken from twelve same-sex littermate genotype trios (one wild-type, one heterozygote, one homozygote from the same litter, six male and six female trios). Brains were removed from 70% ethanol and incubated for three weeks in 8mM gadolinium contrast agent. Brains were then transferred to a 2ml Eppendorf tube filled with Fomblin and scanned in pairs using a three-dimensional gradient echo pulse sequence and an Agilent 7T DirectDrive MRI scanner, with acquisition parameters as follows; matrix 512x192x192 (reconstructed to 512x256x256); field of view 40x10x10 mm; repetition time/echo time (TR/TE) 30/10 ms; 20 signal averages; total scan time 8.2 hours. A 26mm radiofrequency coil was used for signal transmission and reception. Magnetic resonance images were processed blind to genotype using a combination of FSL[2], ANTs[3] and in-house C++ software utilizing the ITK library, available from https://github.com/spinicist/QUIT[4, 5]. In brief, multi-

head scans were bias-field corrected[6] before being split into individual sample images. Registration was then performed between each subject and the Dorr atlas image[7] to ensure all samples were aligned. An average study template image was then constructed using MR images from all animals[8]. The resulting template was then non-linearly registered to the atlas image. All subject images were then non-linearly registered to the study template. The inverse transforms from the atlas to the study template and from the study template to each subject were applied to calculate the total brain volume and individual brain region of interest (ROI) volumes of each subject. ROIs match those found in the Dorr atlas[7].

Histology

Five 9 week old male littermate genotype trios were used for histological analysis except where indicated below. Perfused brains were removed from 70% ethanol and paraffin wax-embedded, then sections were cut from three different zones of the brain; Bregma ≈2.46 (prefrontal cortex); Bregma ≈ 0.75 (lateral ventricles and corpus callosum); Bregma ≈ -1.94 (hippocampus). Brains were processed by the University of Edinburgh Shared University Research Facilities (SURF), using a Leica RM2235 base sledge microtome. Twenty coronal sections of 10µm were cut for each block. Sections were mounted on to Superfrost Plus slides (ThermoFisher Scientific) and oven-dried. Two successive sections were used per location for each procedure.

To visualize cytoarchitecture by Nissl staining, sections were dewaxed in xylene, then rehydrated through graded alcohols. Rehydrated slides were incubated for 2 minutes in 0.2 % Cresyl fast violet solution containing 10 drops of acetic acid per 100 ml. Sections were dehydrated through graded alcohols, then cleared in xylene and cover-slipped with the xylene-based mounting solution DPX (Fisher Scientific).

To examine Parvalbumin-expressing neurons, sections were dewaxed and endogenous peroxidase activity quenched by incubating in methanol containing 1% hydrogen peroxide for 30 minutes. Sections were incubated in 10 mM sodium citrate buffer

at room temperature, then microwaved for 20 minutes at high power. Sections were cooled on ice for 20 minutes, then blocked using 20% normal goat serum (Vector) for 1 hour. Sections were next incubated overnight at 4°C with mouse anti-Parvalbumin primary antibody (Sigma-Aldrich P3088, 1:400 dilution), followed by incubation at room temperature for one hour with biotinylated goat anti-mouse secondary antibody (Sigma-Aldrich, 1:200 dilution). Next, sections were incubated in Vectastain Elite Avidin-Biotin Complex (Vector Laboratories) for 30 minutes before visualization by incubation with 0.05% 3,3'-diaminobenzidine tetrahydrochloride (DAB, Sigma-Aldrich) containing 0.001% hydrogen peroxide. Finally, sections were dehydrated through graded alcohol, cleared in xylene, and cover slipped with DPX. To analyse the distribution of interneurons, the prefrontal cortex sections were initially separated into different regions of interest, distinguished using anatomical features and the Mouse Brain Atlas in stereotaxic coordinates[9], then combined. In the hippocampal sections interneurons were counted in CA1 and the dentate gyrus, as well as the whole hippocampal area. ROIs were set at the same position on each section and the cells were counted manually, blind to genotype, using the Fiji 'Cell Counter' plugin.

To examine apoptotic cells, the same procedure was used except the primary antibody was specific for active (cleaved) caspase-3 (Sigma-Aldrich, AB3623, 1:70 dilution), the secondary antibody was biotinylated goat anti-rabbit (Sigma-Aldrich, 1:200 dilution), with nickel was added to the DAB solution. Sections were counterstained with Nuclear Fast Red (Vector Laboratories).

For cortical layer measurements in barrel cortex, brains were taken from three to five month old mice and immediately placed in 4% paraformaldehyde overnight. Fixed brains were sectioned using a cryostat (Leica) coronally at 50µm from rostral to caudal. Sections were mounted onto Superfrost slides (VWR) in gelatin solution. The slices were washed in acetone and water, then stained in 1% thionin-Nissl and dehydrated in increasing concentrations of alcohol, cleared in xylene and then coverslipped using DPX (Fluka).

Image analysis

For most purposes, images of brain sections were captured using a dotSlide scanner (Olympus). Equivalent areas of both hemispheres were quantified on each slide, blind to genotype, then averaged per animal. Cell density was determined within the regions of interest shown (Supplementary Figure 2), which were manually drawn and set using the Fiji region of interest manager, with area determined and cells counted using the Fiji 'Cell Counter' plugin.

For cortical layer measurements in barrel cortex, brain sections were imaged using a light microscope (Olympus). Barrel cortex could be identified by the presence of barrels in layer IV cortex (Bregma anterior-posterior 0.38 to -1.94mm) whilst sections of brain containing prefrontal cortex (Bregma 2.80 to 2.10mm) were identified using a mouse brain atlas[9]. Analysis of cortical thickness was performed within distinct brain areas. For cortical layer thickness, layers I, II/III, IV and V/IV were measured as distances perpendicular to the pial surface in addition to the total cortical thickness in barrel cortex. Total cortical thickness between the central sulcus and white matter for limbic cortex was measured for prefrontal cortex using Camera Lucida (Olympus).

RNA sequencing

Hippocampi, and cortices minus hippocampus, cerebellum and olfactory bulbs, were dissected from the right brain hemisphere mice at nine weeks of age. Samples were snap frozen in liquid nitrogen and stored at -80^{o}C, then processed in batches of mixed genotypes to extract the RNA. Total RNA samples were assessed with a Fragment Analyser (Agilent) for quality and integrity of total RNA. Libraries were prepared using 100ng of each total RNA sample using the TruSeq Stranded mRNA Library Prep Kit (Illumina). Single end RNA Sequencing was carried out to a depth of approximately 60 to more than 100 million reads. Demultiplexing of sequencing reads was carried out using CASAVA (version 1.8.2, Illumina), with adapters trimmed using Skewer (version 0.1.116)[10]. Raw sequence reads were mapped to mouse reference genome mm10 using STAR (version 2.4.0h)[11].

Raw counts at gene level were obtained using htseq-count[12] (version 0.7.2, in the default union mode) on the alignment bam files and the Ensembl release 85 mouse gtf file. Differential gene expression was analysed using DESeq2 from the R statistical package[13]. Differential exon expression was analysed using DEXSeq[14] (version 1.19.4) using exon counts obtained by running the script "dexseq_count.py" provided by the Deseq package. Adjusted-p-values were calculated via a Benjamini-Hochberg Procedure to get False Discovery Rate (FDR), the default in Deseq2 package. Raw count data for all samples were together subjected to a regularised logarithm transformation[10] using the DESeq2 package version 1.16.1. For each heat map, the transformed counts for each gene were normalised to Z-scores across all samples. Heat maps of gene expression were generated using R (version 3.4.2) and RStudio (version 1.0.143).

Expression-weighted cell-type enrichment (EWCE) analysis

This analysis used the Karolinska Institute 'Superset' of RNASeq profiles generated from six independent single cell RNASeq studies of several brain regions and cell types. The Superset consists of 24 cellular classes generated by hierarchical clustering of nearly 9,970 mouse brain single cell RNASeq profiles (all generated by exactly the same method) followed by cell type identity assignment[15]. Profiles consist of a set of specificity values which provide a measure of gene expression enrichment (calculated from mean expression of each gene in a cellular class divided by its mean expression in all cellular classes) for each gene detected in that class[15]. Some cells were isolated from mouse cortex, hippocampus, striatum, hypothalamus and midbrain, while others were the result of specifically isolating cortical Parvalbumin-positive interneurons or oligodendrocytes from multiple brain regions including somatosensory cortex and hippocampus. The ages of the mice used to generate the profiles include embryonic and a range from P14 to P90. Each class and profile is therefore an amalgamation of single cell profiles from closely related cell

types, not all necessarily from the same brain region or age. Superset profiles were downloaded from http://hjerling-leffler-lab.org/data/scz_singlecell using specificity table: ctd[[1]]$specificity and expression table: ctd[[1]]$mean_exp. Analysis was carried out in the R package using script downloaded from https://github.com/NathanSkene/EWCE/ (version 0.99.2), and default options with Bonferroni multiple testing correction. The full list of expressed *Der1* cortex or hippocampus genes was used as background, as appropriate. The script was run with 10,000 repetitions. The Superset samples were sequenced at a lower depth than the *Der1* samples, and using unique molecular identifiers. Consequently only the most abundantly expressed genes (up to 14,581) were detected. For cortex, 1,794 of 2,125 dysregulated genes are present in the Superset profiles. For hippocampus, 151 of 175 dysregulated genes are present in the Superset profiles. *Der1* whole gene DESeq2 RNASeq data were used for this analysis.

RNASeq deconvolution

RNASeq deconvolution was carried out using the cell Karolinska Institute 'Superset' of RNASeq profiles[15] described above under EWCE analysis as reference. Specificity value thresholds of 0.75 and 0.6 were set to ensure that the most highly enriched genes were used in this analysis, thus profile signatures consisted of genes with at least one specificity value in one cell type above these thresholds. To provide context, specificity value=1 represents 100% specificity for one cell class, the astrocyte marker Gfap exhibits a specificity value of 0.87 in the astrocyte/ependymocyte class, the oligodendrocyte marker Mbp exhibits a specificity value of 0.6 in the oligodendrocyte class, the interneuron marker Parvalbumin exhibits specificity values of 0.41 and 0.27 in the interneuron and striatal interneuron classes, respectively, and the synapse marker Dlg4 (Psd95) exhibits specificity values of ~0.1 in pyramidal neurons and <0.1 in other neuron classes[15]. This resulted in the use of 346 genes for threshold=0.75, and 752 genes for threshold=0.6, of which 285 and 653 are present in our wild-type RNASeq data.

Deconvolution was carried out using CIBERSORT Jar Version 1.06 (May 5th 2017)[16], available at the web interface https://cibersort.stanford.edu. The ability of CIBERSORT to accurately deconvolute the 24 cell types in the Superset was examined by creating artificial cell mixes by combining Superset gene expression values in various proportions from 0 to 0.5. CIBERSORT input was then compared to output to determine the efficiency of artificial sample deconvolution for the 24 cell types.

Pathway analysis

DESeq2 data were examined separately or combined with DEXSeq data by Ingenuity Pathway Analysis (IPA, Qiagen), using corrected p values and log2 fold changes, and the corresponding full list of expressed genes for each brain region as the background gene set. Human t(1;11) translocation neuron RNASeq data[1] were similarly analysed using IPA. Pathway analysis of putative schizophrenia or depression risk genes was carried out using IPA and the full cortical gene expression list as the background gene set. Pathway analysis of dysregulated orthologues of putative schizophrenia or depression risk genes used the corresponding full list of expressed genes for each brain region as the background set. Adjusted $p<0.05$, and $z>2$ or $z<-2$ were used as thresholds throughout. Pathway analysis of dysregulated genes from cell class profiles used the full Superset profile as background. A specificity value threshold of 0.2 was set to ensure that a sufficient number of the most specific genes were used in the analysis. For context regarding specificity values see deconvolution, above. Where DEXSeq identified dysregulated sequences that did not unambiguously map to a single gene, or mass spectrometry identified peptides that could not be unambiguously mapped to a single protein (due to close homology with other proteins), all possible genes and proteins were included in the pathway analysis.

Synaptosome preparation and mass spectrometry

Synaptosomes were prepared from 8-10 week old *Der1* cortex and hippocampus (six wild-type, five heterozygous, five homozygous) as previously described[17]. Tissue was

homogenized in HEPES buffer (5 mM HEPES, pH 7.4, 0.32 M sucrose supplemented with protease inhibitor cocktail, Roche) and centrifuged at 1000 x g for 10 min at 4°C. The supernatant was subsequently centrifuged in a 0.85/1.2 M sucrose gradient at 100,000 x g for 2 hours. Synaptosomes were recovered from the 0.85/1.2 M sucrose interface and concentrated by centrifugation at 18.000 x g for 30 min.

Samples were digested using filter aided sample preparation (FASP) with some modifications[18]. Briefly, 20 µg of each protein sample were incubated with 75 µL 2% SDS, 1 mM Tris(2-carboxyethyl)phosphine at 55°C for 1 hour, after which samples were incubated with 0.5 µL 200 mM methyl methanethiosulfonate for 15 min. Next, 200 µL 8 M Urea in Tris pH 8.8 were added and the samples were transferred to Microcon-30 filter tubes (Millipore). Samples were washed 4 times with 8M Urea in Tris buffer and 4 times with 50 mM ammonium bicarbonate by centrifugation at 14,000 x g for 10 min each. Proteins were digested with 0.7 µg Trypsin/Lys-C Mix (MS grade, Promega) overnight at 37°C. Peptides were eluted with 200 µL 50 mM ammonium bicarbonate, dried in SpeedVac and stored at -20°C.

Peptides were analysed by micro LC MS/MS using an Ultimate 3000 LC system (Dionex, Thermo Scientific) and the TripleTOF 5600 mass spectrometer (Sciex). Peptides were trapped on a 5 mm Pepmap 100 C18 column (300µm i.d., 5µmparticle size, Dionex) and fractionated on a 200 mm AlltimaC18 column (300µm i.d., 3µm particle size). The concentration of acetonitrile in the mobile phase was increased at a flow rate of 5µL/min from 5 to 18% in 88 min, to 25% at 98 min, 40% at 108 min and to 90% in 2 min. Peptides were electro-sprayed into the mass spectrometer with a micro-spray needle (at 5500 V). The mass spectrometer was operated in a data-independent mode, as described in[19]. Each cycle consisted of a parent ion scan of 150 msec and 8 Da MS/MS windows (80 msec scan time each), throughout a 450-770 m/z mass range. The collision energy for each window was calculated for a 2+ ion centered upon the window (spread of 15 eV).

The data were analysed with Spectronaut Pulsar v 12.0.20491.21.28109[20] and using a spectral library created by data-dependent acquisition from hippocampal synapse-enriched

samples containing spike-in iRT peptides (Biognosys). Cross-run normalization was enabled using local normalization strategy. Only peptides quantified with a Q-value ≤ 10^{-2} and 10^{-3} (for hippocampus and cortex datasets, respectively) across all samples in at least two groups were considered. Limma R package was used to Loess normalize protein abundance ('normalizeCyclicLoess' function, 'fast' method and 10 iterations). Volcano plots were generated using R (version 3.6.2). Protein were annotated to synaptic genes and sunburst plots were generated using SynGO 1.0 database and online tool[21].

Hippocampal Cell Culture and Electrophysiological recordings

Primary hippocampal cultures were prepared from individual E17.5 DER littermate pups as described[22]. Briefly, hippocampi were dissected from pups, incubated in Papain, dissociated and grown in Neurobasal A growth medium containing 1% Rat Serum and supplemented with B-27, and maintained until Days In Vitro (DIV) 21.

Whole cell patch clamp recordings were performed as described[23]. Briefly, coverslips containing DIV 21 hippocampal neurons were transferred to a recording chamber with a constant (3-5ml/min) perfusion of external recording solution containing: 150 mM NaCl, 2.8 mM KCl, 10 mM HEPES, 2 mM $CaCl_2$, 10 mM D-glucose and 100 µM glycine, pH 7.35, 320 mOsm. Tetrodotoxin citrate (300 nM) was included to block action-potential driven excitatory events. Patch-pipettes were pulled from borosilicate glass (Harvard Apparatus, Kent, UK) with a resistance of 3-5 MΩ, and filled with a K-gluconate-based internal solution containing: 141 mM Potassium Gluconate, 2.5 mM NaCl, 10 mM HEPES, 11 mM EGTA, pH 7.35). Currents were evoked by S-AMPA (50 µM) and NMDA (150 µM). All currents were recorded at room temperature, using an axopatch 200B amplifier (Molecular Devices, Union City, CA). Neurons were voltage-clamped at -60 mV. Whole-cell currents were analysed using WinEDR v3.2 software (John Dempster, University of Strathclyde, UK), with currents normalised to cell capacitance. For statistical analysis, n was taken as the number of pups, with n=3 WT, 4 HET and 3 HOM. A total of 12 WT, 14 HET and 11 HOM genotype coverslips were recorded from.

Statistical analysis

For analysis of MRI data, a multivariate general linear model 2-way MANCOVA statistical test was performed using SPSS statistics 22 (IBM) to determine group-level differences in brain ROI volumes with genotype as fixed effect, total brain volume and brain region as dependent variable, and littermate trio groupings as covariate.

For enrichment analysis, hypergeometric probabilities were calculated using keisan.casio.com/exec/system/1180573201. As with the pathway analysis, where DEXSeq identified dysregulated sequences that did not unambiguously map to a single gene, or mass spectrometry identified peptides that could not be unambiguously mapped to a single protein (due to close homology with other proteins), all possible genes and proteins were included in the enrichment analysis.

For the proteomic analysis, empirical Bayes moderated t-statistics with multiple testing correction by false discovery rate were performed on log-transformed protein abundances ('eBayes' and 'topTable' functions from Limma R package), as previously described[18, 19, 24, 25]. Proteins with a FDR adjusted p-value < 0.05 were considered significantly regulated for subsequent downstream analysis.

Other statistical analyses were carried out using GraphPad Prism, with statistical tests used stated in figure legends.

Supplementary Table 1 (Excel file) Magnetic resonance imaging data. Both hemispheres, regional volumes (mm^3) corrected to individual whole brain volumes, left and right hemispheres combined, separate hemispheres, regional volumes (mm^3) corrected to individual whole brain volumes, left and right hemispheres considered separately

Supplementary Table 2 (Excel file) RNA sequencing data. **a** DeSeq2 (whole gene differential expression) *Der1* cortex data, **b** DEXSeq (exon level differential expression) *Der1*

cortex data, **c** DeSeq2 (whole gene differential expression) *Der1* hippocampus data, **d** DEXSeq (exon level differential expression) *Der1* hippocampus data. In each case data are provided with comparisons to human IPSC-derived cortical neuron cultures from members of the t(1;11) family[12], two large-scale genome-wide association studies of schizophrenia[1, 2], synapse genes from a large-scale schizophrenia CNV study[3], two large-scale genome-wide association studies of depression[4, 6], a large-scale genome-wide association study of bipolar disorder[5], a large-scale genome-wide association study of Alzheimer's Disease[55] where matches were found, and a large-scale genome-wide association study of cerebral cortex architecture[65], where matches were found (references numbered according to main text). Overlaps are represented by a gene name in the relevant genetic study column. Non-overlaps are represented by empty cells, BaseMean, mean of normalised counts of all samples; p value, p value for wild-type versus heterozygous; adjusted p value, p value adjusted for multiple testing

Supplementary Table 3 (Excel file) Dysregulated genes with conserved cAMP response elements according to http://natural.salk.edu/creb/.

Supplementary Table 4 (Excel file) Ingenuity Pathway Analysis functions. **a** functions enriched for dysregulated genes in *Der1* cortex. All functions in the categories 'Molecular and cellular function' and 'Physiological system development and function' are included. Selected top relevant functions are provided in Table 1. Data are provided with comparisons to functions predicted from human IPSC-derived cortical neuron cultures from members of the t(1;11) family[12] (reference numbered according to main text). Overlaps are represented by an x in the human neuron column. Non-overlaps are represented by empty cells, **b**, functions enriched for dysregulated genes in *Der1* hippocampus. All functions in the categories 'Molecular and cellular function' and 'Physiological system development and function' are included. Selected top relevant functions are provided in Supplementary Table

5. **c**, functions enriched for dysregulated genes in Superset cell classes. All functions in the categories 'Molecular and cellular function' and 'Physiological system development and function' are included. Selected top relevant functions are provided in Supplementary Table 6. **d**, functions enriched for dysregulated genes in human IPSC-derived cortical neuron cultures from members of the t(1;11) family. All functions in the categories 'Molecular and cellular function' and 'Physiological system development and function' are included. Selected top relevant functions are provided in Table 1. The genes listed for each function are dysregulated in the corresponding dataset.

Supplementary Table 5 Top predicted relevant altered functions in heterozygous *Der1* mouse hippocampus.

Function (no. of molecules[a])	***Der1* hippocampus score (no. of genes[b])**
General cell morphology	
Development of neurons (1,423)	p=2e-9 (33)
Morphology of neurons (1,123)	p=8e-7 (22)
Maturation of neurons (114)	p=8e-6 (7)
Abnormal morphology of neurons (923)	p=3e-5 (16)
Differentiation of neurons (648)	p=5e-4 (14)
Cell contact	
Adhesion of neuronal cells (89)	p=8e-9 (9)
Formation of plasma membrane (406)	p=1e-8 (17)
Cell-cell contact (1,118)	p=1e-5 (22)
Cell-cell contact of neurons (24)	p=1e-5 (4)
Cell-cell adhesion of neurons (22)	p=3e-4 (3)
Cytoskeleton	
Microtubule dynamics (2,247)	p=2e-4 (31)
Organization of cytoskeleton (2,624)	p=7e-4 (33)
Cellular protrusions/neurites	
Neuritogenesis (1,067)	p=2e-6 (23)
Formation of cellular protrusions (1,645)	p=1e-4 (26)
Growth of neurites (910)	p=2e-4 (16)
Branching of cells (746)	p=2e-4 (14)
Extension of neurites (267)	p=5e-4 (8)
Axons	
Extension of axons (134)	p=5e-3 (5)
Myelination of optic nerve (8)	p=2e-3 (2)
Myelination (8)	p=5e-3 (7)
Dendrites	
Formation of dendrites (209)	p=2e-4 (8)
Dendritic growth/branching (446)	p=4e-4 (10)
Density of dendritic spines (143)	p=1e-3 (5)
Morphology of dendrites (138)	p=3e-3 (5)
Length of dendrites (47)	p=3e-3 (3)
Cell proliferation	
Proliferation of epithelial cells (996)	p=3e-3 (14)
Neurogenesis of cerebral cortex (69)	p=5e-3 (3)
Proliferation of stem cells (372)	p=8e-3 (7)
Transport	
Exocytosis (336)	p=9e-4 (8)
Transport of dopamine (76)	p=8e-4 (3)
Secretion of neurotransmitter (248)	p=1e-3 (7)
Release of neurotransmitter (510)	p=1e-3 (7)
Transport of 5-hydroxytryptamine (40)	p=2e-3 (2)
Neurotransmission	
Developmental process of synapse (303)	p=3e-9 (16)
Neurotransmission (716)	p=8e-8 (20)
Synaptic transmission (558)	p=3e-7 (17)
Maturation of synapse (36)	p=3e-5 (4)
Miniature excitatory postsynaptic currents (71)	p=2e-4 (5)
Plasticity of synapse (170)	p=3e-4 (7)
Excitatory postsynaptic potential (166)	P=3e-4 (7)
Paired-pulse facilitation of synapse (55)	p=9e-4 (4)
Action potential of cells (238)	p=1e-3 (7)
Formation of excitatory synapses (14)	p=3e-3 (2)

A full list of functions is provided in Supplementary Table 4b. Related functions are grouped, with top functions shown for each group. a, total number of molecules relating to each IPA function; b, number of dysregulated genes relating to each function

Supplementary Table 6 Top predicted relevant altered cellular functions in cell classes from EWCE analysis.

Superset cell class	
Function (no. of molecules[a])	***Der1* cortex score (no. of genes[b])**
***Der1* cortex pyramidal CA1**	
Long-term potentiation (539)	p=6e-6 (8)
Neurotransmission (773)	p=5e-5 (9)
Excitation of cerebral cortex cells (46)	p=6e-5 (3)
Synaptic transmission (601)	p=6e-5 (8)
Excitation of neurons (167)	p=9e-5 (4)
Remodelling of F-actin structure (7)	p=1e-4 (2)
Development of neurons (1,474)	p=2e-4 (12)
Neuritogenesis (1,110)	p=3e-4 (10)
AMPA mediated synaptic current (9)	p=3e-4 (2)
Activation of neurons (252)	p=3e-4 (4)
***Der1* cortex pyramidal somatosensory**	
Efflux of dopamine (63)	p=2e-5 (3)
Quantity of dense core vesicles	p=2e-4 (2)
Neurotransmission (773)	p=3e-4 (9)
Synaptic transmission 601)	p=3e-4 (8)
Exocytosis by eukaryotic cells (99)	p=1e-3 (3)
Fusion of synaptic vesicles (21)	p=1e-3 (2)
Action potential of neurons (198)	p=3e-3 (4)
Quantity of synapse (92)	p=3e-3 (3)
Accumulation of cortical actin filaments (1)	p=4e-3 (1)
Activation of parvocellular neurons (1)	p=4e-3 (1)
***Der1* cortex interneurons**	
Neurotransmission (773)	p=7e-6 (7)
Activation of neurons (252)	p=1e-5 (4)
Action potential of neurons (198)	p=5e-5 (4)
Excitation of neurons (167)	p=2e-4 (3)
GABA-mediated receptor currents (14)	p=2e-4 (2)
Fusion of plasma membrane (34)	p=4e-4 (2)
Excitation of cerebral cortex cells (46)	p=5e-4 (2)
Activation of enzyme (584)	p=9e-4 (5)
Accumulation of 2-arachidonoylglycerol (3)	p=1e-3 (1)
Activation of parvocellular neurons (1)	p=1e-3 (1)
***Der1* cortex astrocytes/ependymocytes**	
Fatty acid metabolism (1,492)	p=3e-8 (17)
Concentration of lipid (2,135)	p=3e-7 (19)
Uptake of amino acids (264)	p=8e-7 (6)
Uptake of glutamine family amino acid (133)	p=9e-7 (5)
Function of neuroglia (56)	p=2e-6 (5)
Mass of fat (24)	p=2e-6 (4)
Transport of amino acids (394)	p=3e-6 (7)
Concentration of fatty acid (721)	p=4e-6 (10)
Function of central nervous system (152)	p=4e-6 (6)
Function of oligodendrocytes (9)	p=5e-6 (3)

A full list of functions is provided in Supplementary Table 5c, e. The most highly enriched genes that are dysregulated in *Der1* cortex for each cell class were used for IPA analysis, with specificity value cut-off=0.2 (SV=1 indicates 100% specificity, see methods for more context). In many cell classes the relatively low number of genes above this threshold was

insufficient for meaningful pathway analysis. a, total number of molecules relating to each IPA function; b, number of dysregulated genes relating to each function

Supplementary Table 7 (Excel file) Synaptosome mass spectrometry data. **a**, Mass spectrometry analysis of cortex synaptosomes isolated from wild-type (WT), heterozygous (HET) or homozygous (HOM) *Der1* mice, **b**, Mass spectrometry analysis of hippocampus synaptosomes isolated from wild-type (WT), heterozygous (HET) or homozygous (HOM) *Der1* mice, **c**, SynGo annotations. SD, standard deviation

Supplementary table 8 Comparison between characteristics of the *Der1* mouse and pertinent characteristics of mutant mice that are known or proposed to be relevant to the t(1;11) translocation.

Mutant	Brain structure	Synapses & plasticity	Electrophysiology	Neuronal intracellular transport
Der1	↑ hippocampal Parvalbumin-positive interneuron density altered oligodendrocyte-myelin function[26] no gross structural changes	↑ surface/synaptic NMDA receptor expression in cultured hippocampal neurons[1] altered Psd95 distribution indicative of an increased density of weaker synapses[1] altered expression of genes involved in synapse formation, structure & function altered expression of genes critical for synaptic plasticity and long-term potentiation, including the CREB signalling pathway	↓ AMPA/NMDA ratio in cultured hippocampal neurons	↑ NMDA receptor motility[1] altered expression of genes required for vesicle transport and exo/endocytosis
humanised DISC1-Boymaw & Boymaw-DISC1[27] endogenous mouse *Disc1* gene replaced with human *DISC1-Boymaw* or *Boymaw-DISC1* cDNA fusion transgenes (*Boymaw* is otherwise known as *DISC1FP1*) resulting in *Disc1* promoter-driven forced expression of putative chimeric proteins[28] (whose expression in t(1;11) carriers remains to be established[1])		↓ cortical expression of NMDA receptor subunit GluN1 and Psd95[27]		
Disc1Δ2-3[29] deletion of exons 2 & 3 from endogenous mouse *Disc1* gene, abolishes full-length Disc1 expression	↓ density of Parvalbumin-positive interneurons in many cortical areas[30], and in hippocampus[31] no gross structural changes[29]	catecholaminergic network dysfunction[32] ↓ methamphetamine-induced dopamine release & ↑ dopamine receptor expression in nucleus accumbens[31]	↑ threshold for induction of long-term potentiation in hippocampus[29]	↓ dendritic ITPR1 mRNA transport in cultured hippocampal neurons[33] ↓ synaptic vesicle exocytosis[34]
Disc1-LI[35] deletion of exons 1-3 from endogenous mouse *Disc1* gene, abolishes full-length Disc1 expression			altered parvalbumin-positive interneuron function[36]	
$Disc1_{tr}$[37] C-terminally truncated Disc1 (encoded by exons	↓ density of Parvalbumin-positive interneurons in hippocampus and medial prefrontal	↓ NMDA receptor GluN2A & GluN2B, ↑ GluN1 (trend) protein expression in hippocampus[38]	↑ long-term potentiation in Schaffer collateral commissural pathway temporoammonic long-term potentiation	

1-8) fused to green fluorescent protein, expressed from transgenic mouse bacterial artificial chromosome under control of *Disc1* promoter	cortex, and displacement in dorsolateral prefrontal cortex[37] ↑ lateral ventricle volume ↓ cerebral cortex thickness partial agenesis of corpus callosum[37]		abolished[39] altered hippocampus-prefrontal cortex connectivity & reduced neurotransmitter release probability in the glutamatergic hippocampal CA1–prefrontal cortex projection[38]	
hDISC1[40] C-terminally truncated DISC1 (exons 1-8) transgene under inducible control of CaMKII promoter	↓ density of Parvalbumin-positive cortical interneurons[41] ↑ lateral ventricle volume[40] altered oligodendrocyte specification[42, 43]	↓ cortical dopamine[41] & dopamine D2 receptor binding in olfactory tubercle and nucleus accumbens (trend)[44] ↑ dendritic spine density[41] ↑ vesicular glutamate transporters in astrocytes[45] ↑ NMDA receptor subunit GluN1, ↓ GluN2A in hippocampus[45] altered homeostasis of dopamine and glutamate receptors in the nucleus accumbens[46] reduced capacity of astrocytes to support dendritic and synaptic development[47]	↑ spontaneous excitatory postsynaptic currents in cultured cortical neurons[48]	altered expression of proteins required for vesicular transport[49]
DN-DISC1[50] C-terminally truncated DISC1 (exons 1-8) transgene under control of CamKII promoter	↓ density of Parvalbumin-positive cortical interneurons[50] ↑ lateral ventricle volume[50]		oscillations in hippocampal CA1[51] abnormal action potentials, and dopaminergic regulation, in fast spiking parvalbumin-positive interneurons of prefrontal cortex[52]	
DN-DISC1-PrP[53] C-terminally truncated DISC1 (exons 1-8) transgene under control of PrP promoter	no gross structural changes[53]			
nes-DN-DISC1[54] C-terminally truncated DISC1 (exon 1-8) transgene inducibly expressed in neural precursor cells	↑ density of Parvalbumin-positive interneurons in cingulate cortex, retrosplenial granular cortex, and motor cortex[54]			
Disc1^{Tm1Kara} [55] natural deletion within mouse Disc1	Parvalbumin-positive interneuron density unchanged[56]	↓ dendritic spine density & altered spine morphology in cultured hippocampal and	↓ short-term potentiation at hippocampal CA1-CA3 synapse	↓ synaptic vesicle volume at hippocampal CA3 synapses[58]

exon 6 that introduces a premature termination codon, combined with targeted premature transcription termination signal in intron 8, abolishes full-length Disc1 expression and may express C-terminally truncated protein due to the termination codon within exon 7	↓ prefrontal cortex volume[56]	cortical neurons[57] altered hippocampal CREB signalling[58]	altered short-term plasticity at mossy fibre-CA3 circuit[58] ↑ neuronal excitability in medial prefrontal cortex[59] ↑ short-term depression & probable ↑ neurotransmitter release probability in medial prefrontal cortex[59] ↑ spontaneous excitatory postsynaptic currents in cultured cortical neurons[48] altered spontaneous inhibitory postsynaptic currents in cultured cortical neurons[48]	proteomic changes suggest effects upon synaptic vesicle transport[59]

The mutants fall into three main categories 1) recapitulation of the gene fusion between *DISC1* and *DISCFP1* (*Der1*, transgenic *Boymaw* fusions), 2) elimination of full-length *Disc1* expression (*Der1*, transgenic *Boymaw* fusions, Disc1△2-3, DISC1-LI, $Disc1^{Tm1Kara}$), 3) transgenic overexpression of a truncated form of *Disc1* or *DISC1* encoded by exons 1-8 that was inferred to arise from the t(1;11) prior to discovery of the *DISC1*/*DISCFP1* gene fusion ($Disc1_{tr}$, hDisc1, DN-DISC1, DN-DISC1-PrP, nes-DN-DISC1).

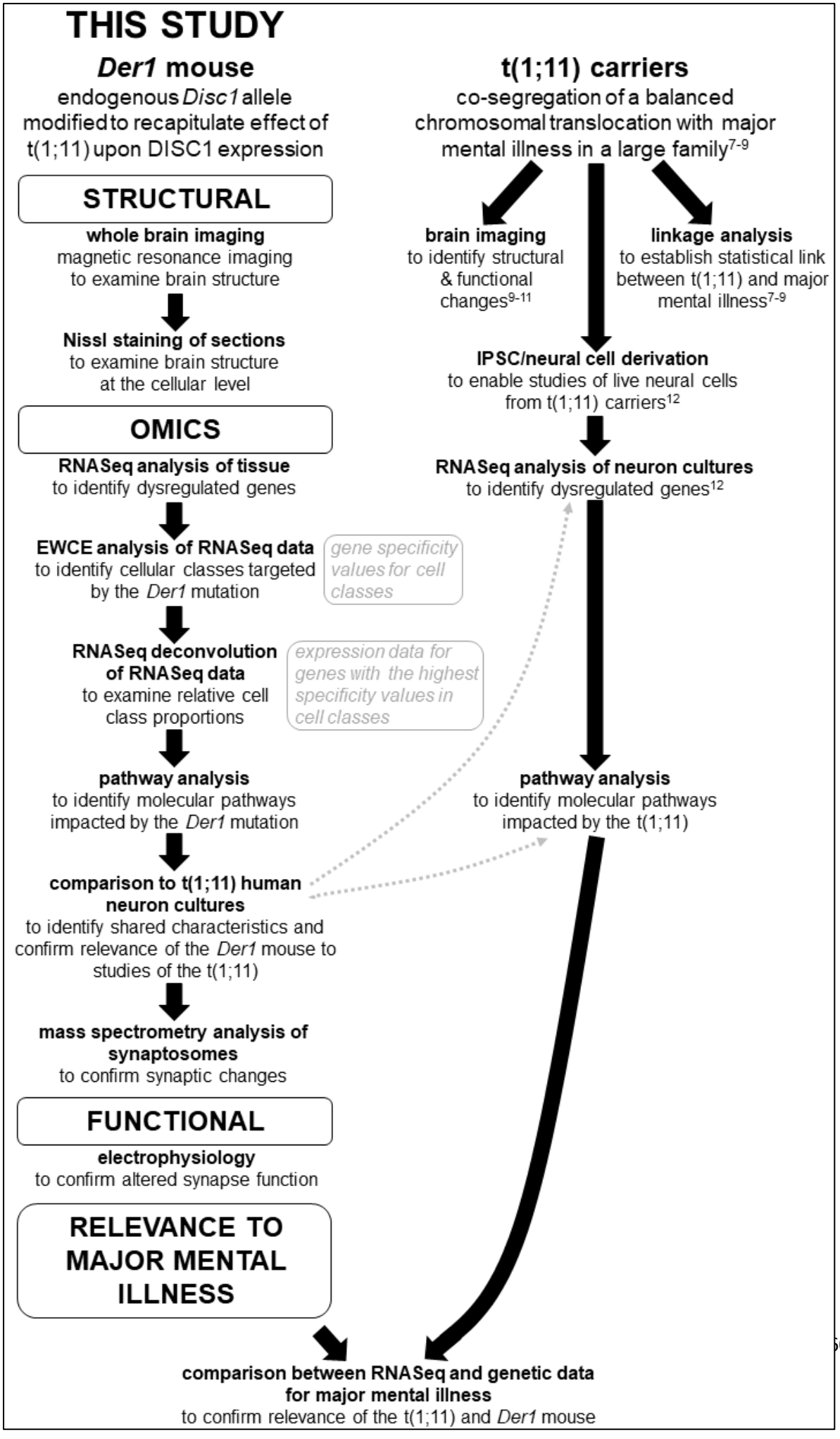
THIS STUDY
Der1 mouse
endogenous Disc1 allele modified to recapitulate effect of t(1;11) upon DISC1 expression
t(1;11) carriers
co-segregation of a balanced chromosomal translocation with major mental illness in a large family[7-9]
STRUCTURAL
whole brain imaging
magnetic resonance imaging to examine brain structure
Nissl staining of sections
to examine brain structure at the cellular level
brain imaging
to identify structural & functional changes[9-11]
linkage analysis
to establish statistical link between t(1;11) and major mental illness[7-9]
IPSC/neural cell derivation
to enable studies of live neural cells from t(1;11) carriers[12]
OMICS
RNASeq analysis of tissue
to identify dysregulated genes
RNASeq analysis of neuron cultures
to identify dysregulated genes[12]
EWCE analysis of RNASeq data
to identify cellular classes targeted by the Der1 mutation
gene specificity values for cell classes
RNASeq deconvolution of RNASeq data
to examine relative cell class proportions
expression data for genes with the highest specificity values in cell classes
pathway analysis
to identify molecular pathways impacted by the Der1 mutation
pathway analysis
to identify molecular pathways impacted by the t(1;11)
comparison to t(1;11) human neuron cultures
to identify shared characteristics and confirm relevance of the Der1 mouse to studies of the t(1;11)
mass spectrometry analysis of synaptosomes
to confirm synaptic changes
FUNCTIONAL
electrophysiology
to confirm altered synapse function
RELEVANCE TO MAJOR MENTAL ILLNESS
comparison between RNASeq and genetic data for major mental illness
to confirm relevance of the t(1;11) and Der1 mouse

Supplementary Fig. 1 Flowchart indicating the experimental approach taken. Superscript numbers indicate references according to the main (not supplementary) text.

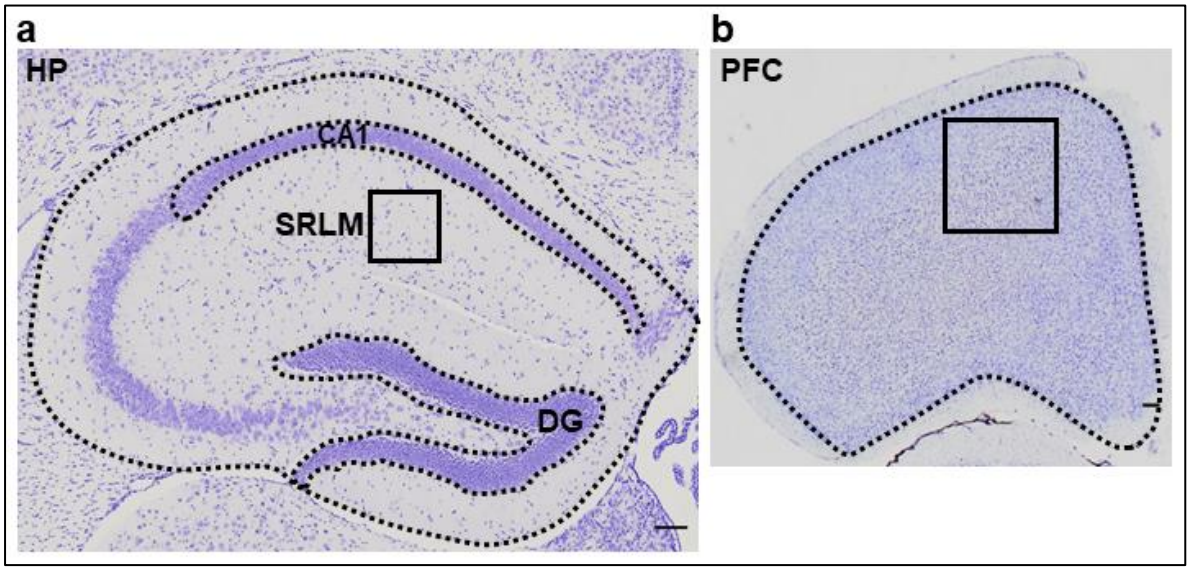

Supplementary Fig. 2 Regions of interest for image analysis of cell density, Parvalbumin and cleaved Caspase 3. **a** Hippocampus (HP). The box indicates the region of the Stratum, Radiatum, Lacunosum and Moleculare (SRLM) in which cell density was quantified. Dotted lines outline the hippocampal formation, CA1 and the dentate gyrus (DG) used for quantification of Parvalbumin-positive cells and cells expressing cleaved Caspase 3. **b** Prefrontal cortex (PFC). The box indicates the region in which cell density was quantified. The dotted line outlines the region in which Parvalbumin-positive cells and cells expressing cleaved Caspase 3 were quantified. Scale bars, 100μm

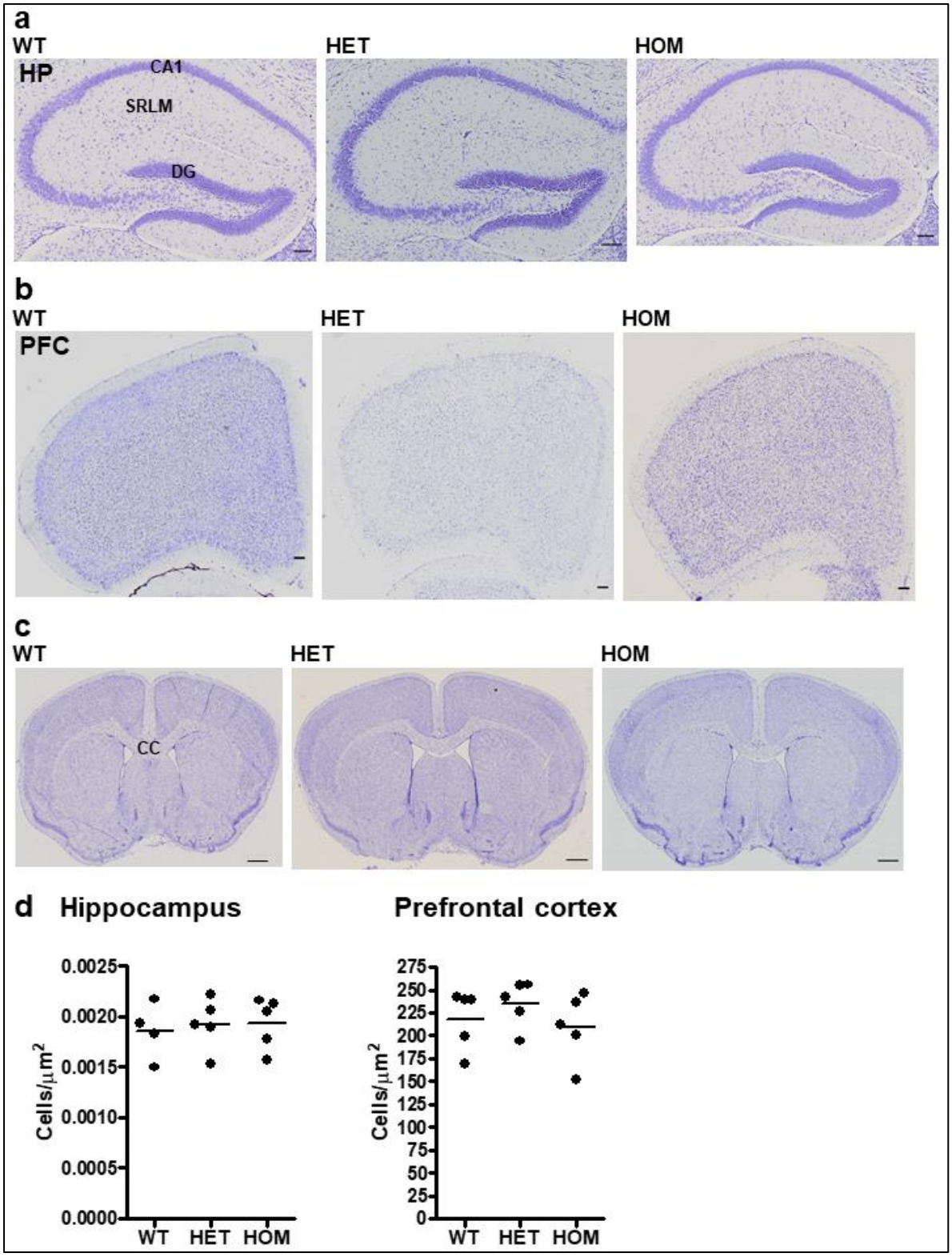

Supplementary Fig. 3 Brain structure visualised by Nissl staining. Sections through hippocampus (HP) **a**, prefrontal cortex (PFC) **b**, and corpus callosum (CC) **c**, were stained with Nissl to visualise cell bodies and tissue structure. scale bars, 100μm in a and b, 500μm in c **d** Quantification of average cell density from both sides of the brain in hippocampal

Stratum, Radiatum, Lacunosum and Moleculare, and PFC. Data were analysed by Kruskal-Wallis one-way ANOVA. Horizontal line on graphs, average of values for each sample; WT, wild-type; HET, heterozygous *Der1*; HOM, homozygous *Der1*

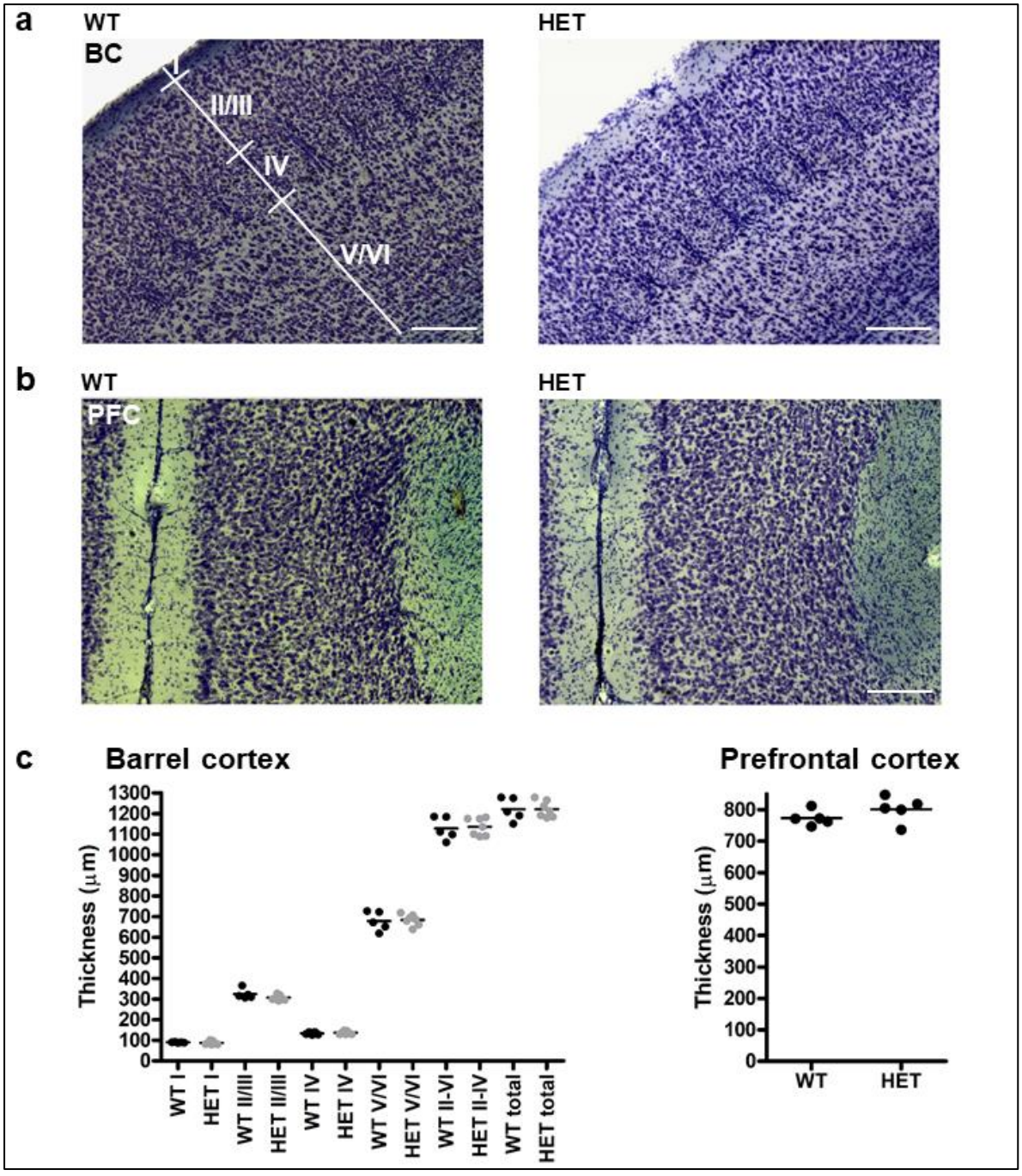

1354

1355 **Supplementary Fig. 4** Cortical layers visualised by Nissl staining. Barrel cortex was used to
1356 examine layering in detail because the individual cortical layers could not be distinguished in
1357 prefrontal cortex. Sections through barrel cortex (BC) **a**, and prefrontal cortex (PFC) **b**, were
1358 stained with Nissl to visualise cell bodies and tissue structure. Cortical layers and
1359 measurements taken are indicated. **c** Quantification of layer thickness in barrel cortex and
1360 PFC. Two-way ANOVA found no effect of genotype on layer thickness ($F_{1,40}$=0.1959,
1361 p>0.05), nor any interaction between layer thickness and genotype ($F_{3,40}$= 0.6631, p>0.05) in

barrel cortex. Unpaired two-tailed t-test found no effect of genotype on cortical thickness in PFC ($p=0.2$). Horizontal line on graphs, average of values for each sample; scale bars, 200μm; WT, wild-type; HET, heterozygous *Der1*

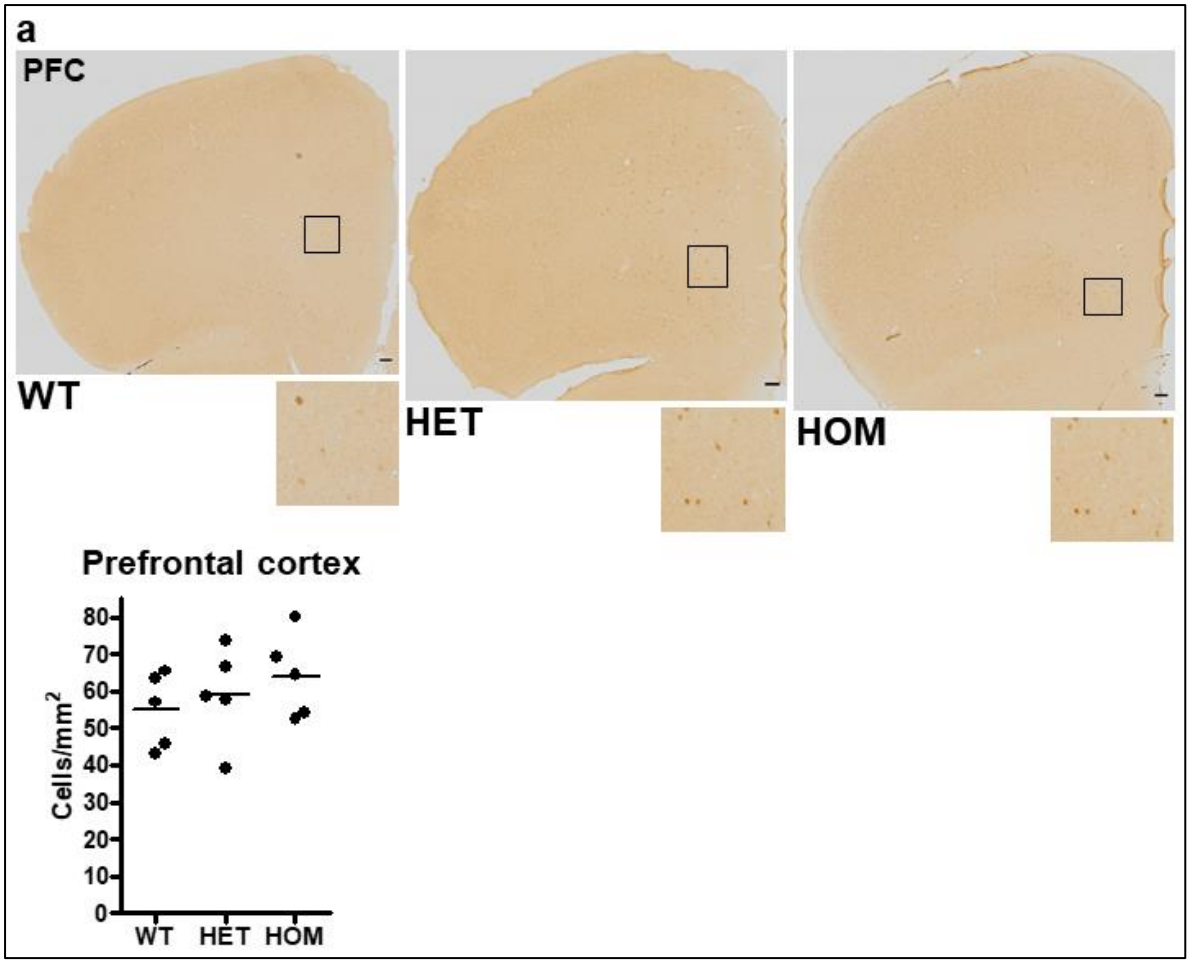

1365

1366 **Supplementary Fig. 5** No change in Parvalbumin-expressing interneuron density in *Der1*
1367 prefrontal cortex. **a** Prefrontal cortex (PFC) sections from nine week old mouse brain were
1368 stained with an antibody specific for Parvalbumin. Enlarged regions showing Parvalbumin-
1369 expressing interneurons are indicated by boxes. scale bars, 100μm **b** Average density of
1370 Parvalbumin-expressing interneurons from both sides of the brain. Data were analysed by
1371 Kruskal-Wallis one-way ANOVA. Horizontal line on graphs, average of values for each
1372 sample; WT, wild-type; HET, heterozygous *Der1*; HOM, homozygous *Der1*

1373

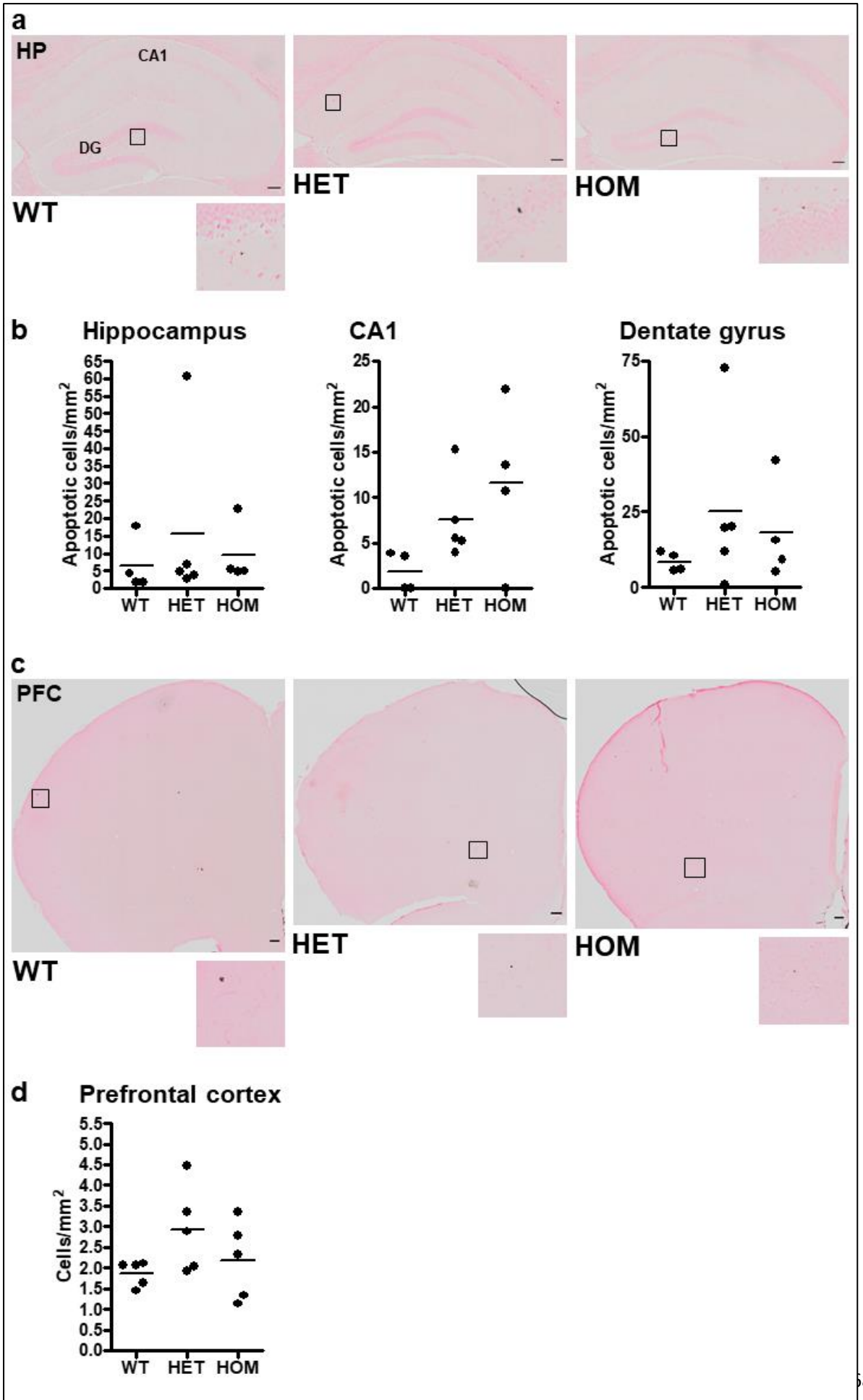
a
HP
CA1
DG
WT
HET
HOM
b
Hippocampus
CA1
Dentate gyrus
Apoptotic cells/mm2
WT
HET
HOM
c
PFC
WT
HET
HOM
d
Prefrontal cortex
Cells/mm2
WT
HET
HOM

Supplementary Fig. 6 Quantification of apoptotic cells. **a** Hippocampal (HP) sections from nine week old mouse brain were stained with an antibody specific for Activated Caspase 3 and counterstained with Nuclear Fast Red. Enlarged regions showing apoptotic cells are indicated by white boxes. **b** Average density of hippocampal apoptotic cells from both sides of the brain. Hippocampus refers to the whole hippocampal formation. **c** Prefrontal cortex (PFC) sections from nine week old mouse brain were stained with an antibody specific for Activated Caspase 3 and counterstained with Nuclear Fast Red. Enlarged regions showing apoptotic cells are indicated by boxes. **d** Average density of PFC apoptotic cells from both sides of the brain. Data were analysed by Kruskal-Wallis one-way ANOVA, p=0.06 for CA1. Horizontal line on graphs, average of values for each sample; WT, wild-type; HET, heterozygous *Der1*; HOM, homozygous *Der1*; DG, dentate gyrus; scale bars, 100μm

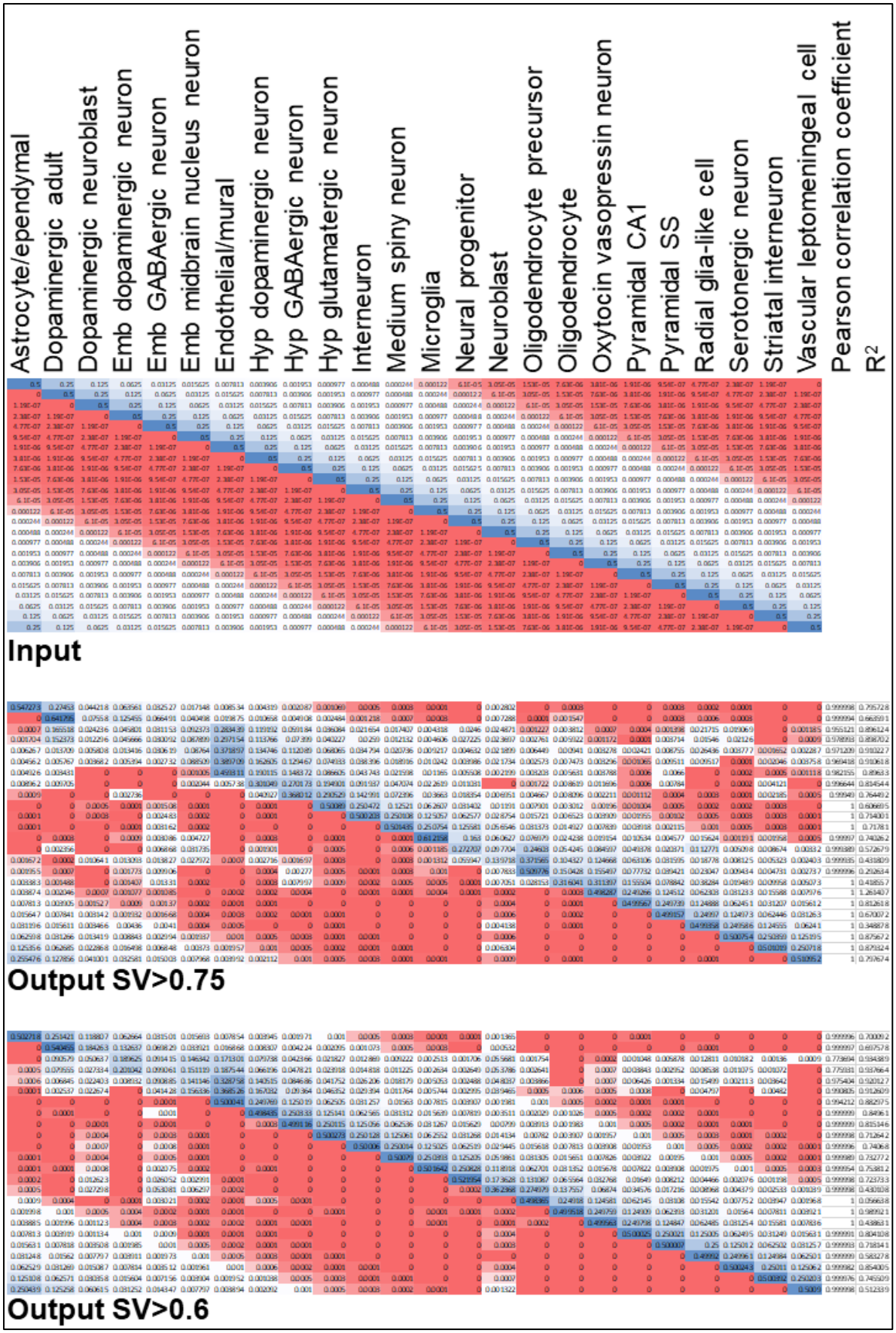
Astrocyte/ependymal
Dopaminergic adult
Dopaminergic neuroblast
Emb dopaminergic neuron
Emb GABAergic neuron
Emb midbrain nucleus neuron
Endothelial/mural
Hyp dopaminergic neuron
Hyp GABAergic neuron
Hyp glutamatergic neuron
Interneuron
Medium spiny neuron
Microglia
Neural progenitor
Neuroblast
Oligodendrocyte precursor
Oligodendrocyte
Oxytocin vasopressin neuron
Pyramidal CA1
Pyramidal SS
Radial glia-like cell
Serotonergic neuron
Striatal interneuron
Vascular leptomeningeal cell
Pearson correlation coefficient
R2
Input
Output SV>0.75
Output SV>0.6

1386

Supplementary Fig. 7 Test deconvolution of the 24 Superset cell classes[15]. Reference profiles were generated using stringent specificity value (SV) thresholds of 0.75 or 0.6 to ensure that each cell class was represented by its most specific genes. *In silico* samples were created by mixing the thresholded gene expression profiles in proportions between 0 and 0.5. CIBERSORT input was compared to output and Pearson correlation coefficient and R^2 calculated to assess the quality of deconvolution of each artificial sample.

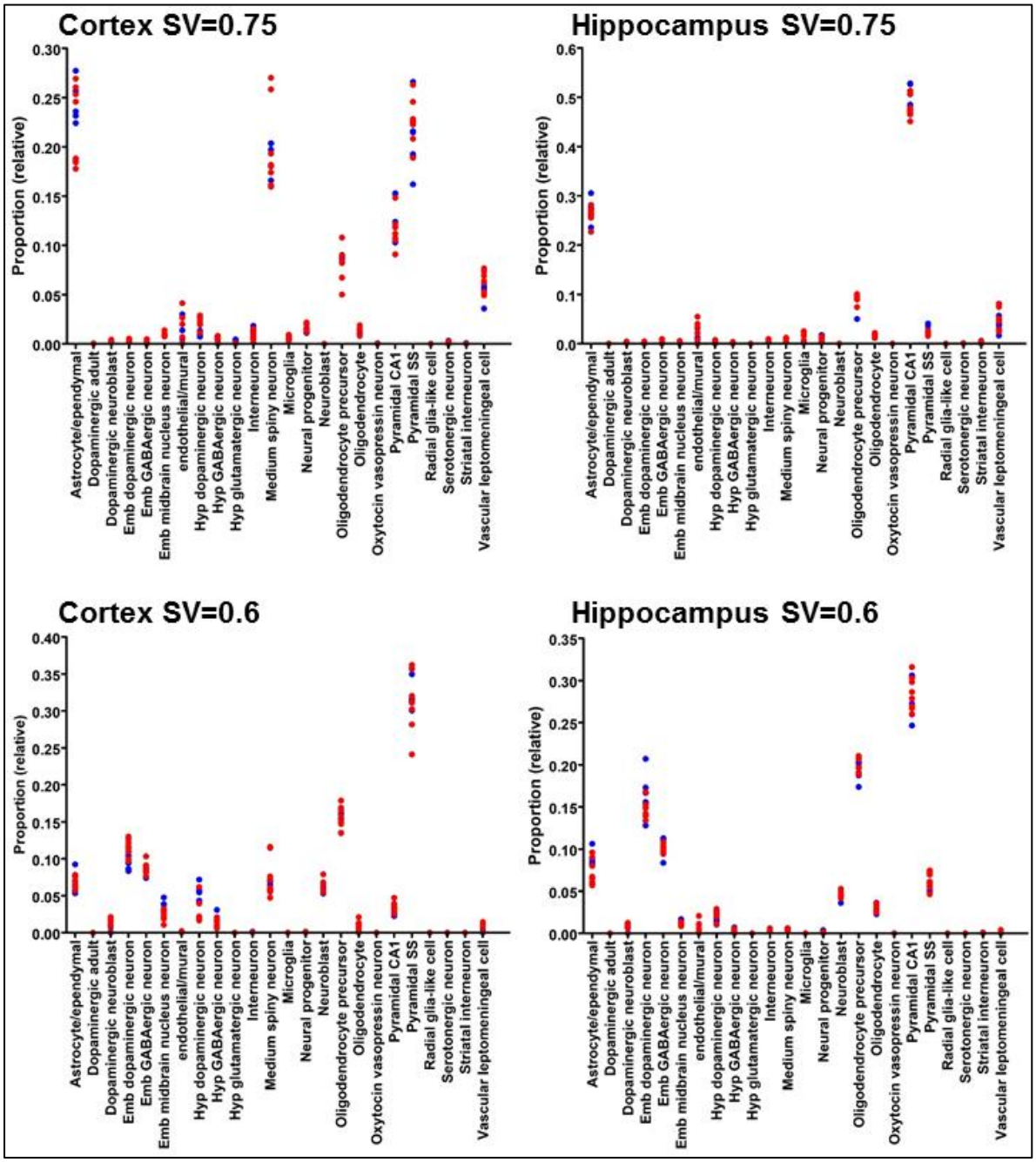

Supplementary Fig. 8 Deconvolution of heterozygous *Der1* cortex and hippocampus RNASeq data using the Superset cell class profiles[15] as reference. Reference profiles were generated using stringent specificity value (SV) thresholds of 0.75 or 0.6 to ensure that each cell class was represented by its most specific genes. Note that although the proportions change with the threshold set, and therefore the number of specific genes used for deconvolution, the relative proportions of each cell class do not differ between genotypes.

Samples from embryonic cell types, neural progenitors and neuroblasts were not accurately deconvolved by CIBERSORT, thus their apparently high levels in the wild-type and *Der1* tissue are not an indication of true prevalence. Blue, wild-type; red, *Der1* heterozygote; Emb, embryonic

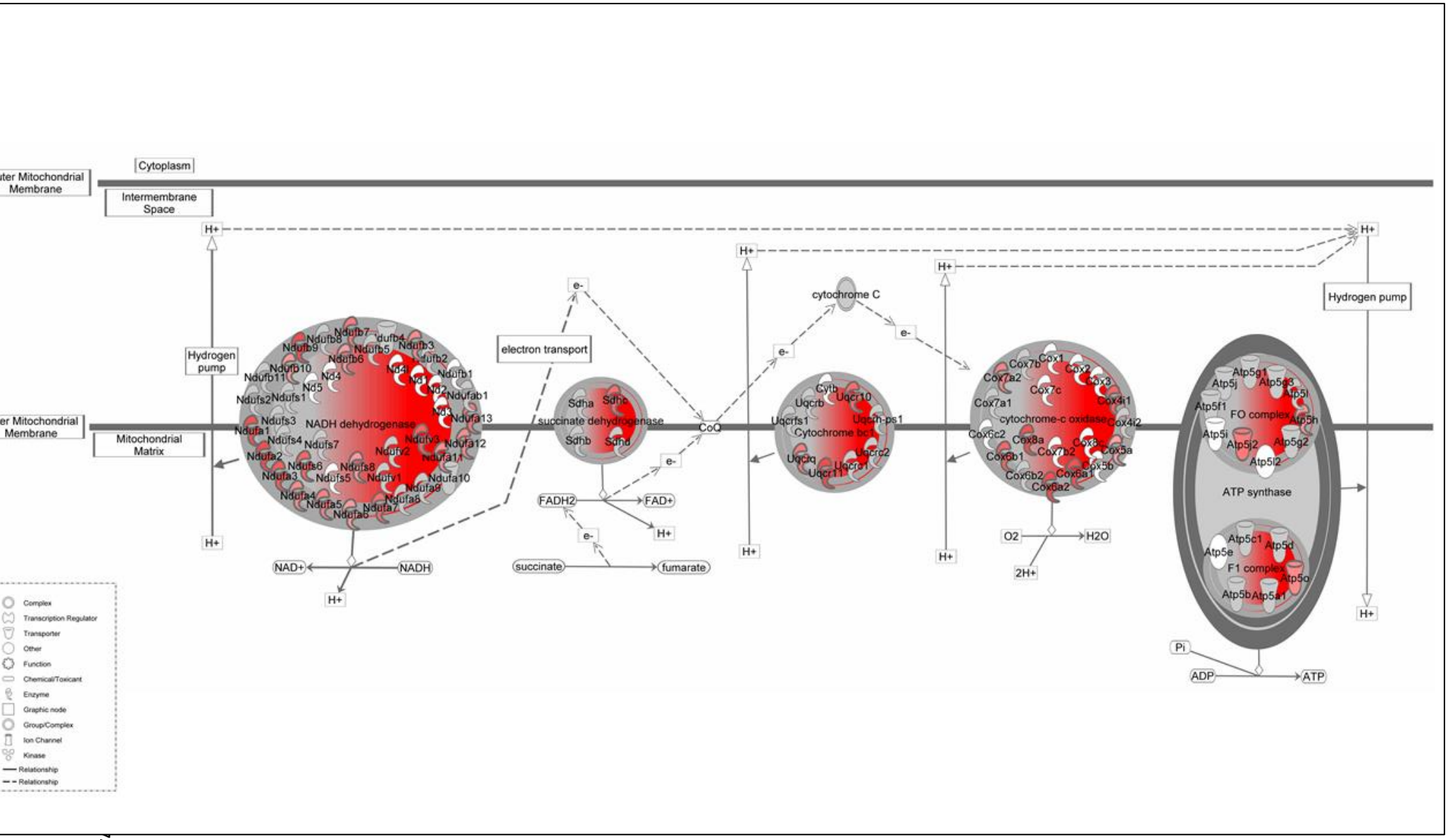
Cytoplasm
Intermembrane Space
Mitochondrial Matrix
Hydrogen pump
electron transport
Hydrogen pump
NADH dehydrogenase
succinate dehydrogenase
cytochrome C
Cytochrome bc1
cytochrome-c oxidase
ATP synthase
FO complex
F1 complex
CoQ
NAD+
NADH
FADH2
FAD+
succinate
fumarate
O2
H2O
2H+
Pi
ADP
ATP
H+
e-
Complex
Transcription Regulator
Transporter
Other
Function
Chemical/Toxicant
Enzyme
Graphic node
Group/Complex
Ion Channel
Kinase
Relationship
Relationship

Supplementary Fig. 9 *Der1* cortex gene dysregulation within the 'Oxidative phosphorylation' canonical pathway. Pathway impairment was predicted by IPA based on gene dysregulation at the whole gene level using DESeq2 data. Double outlines indicate protein complexes, the components of which can be found in Supplementary Table 2a, b. Colour intensity represents strength of gene expression change. green, downregulated; red, upregulated

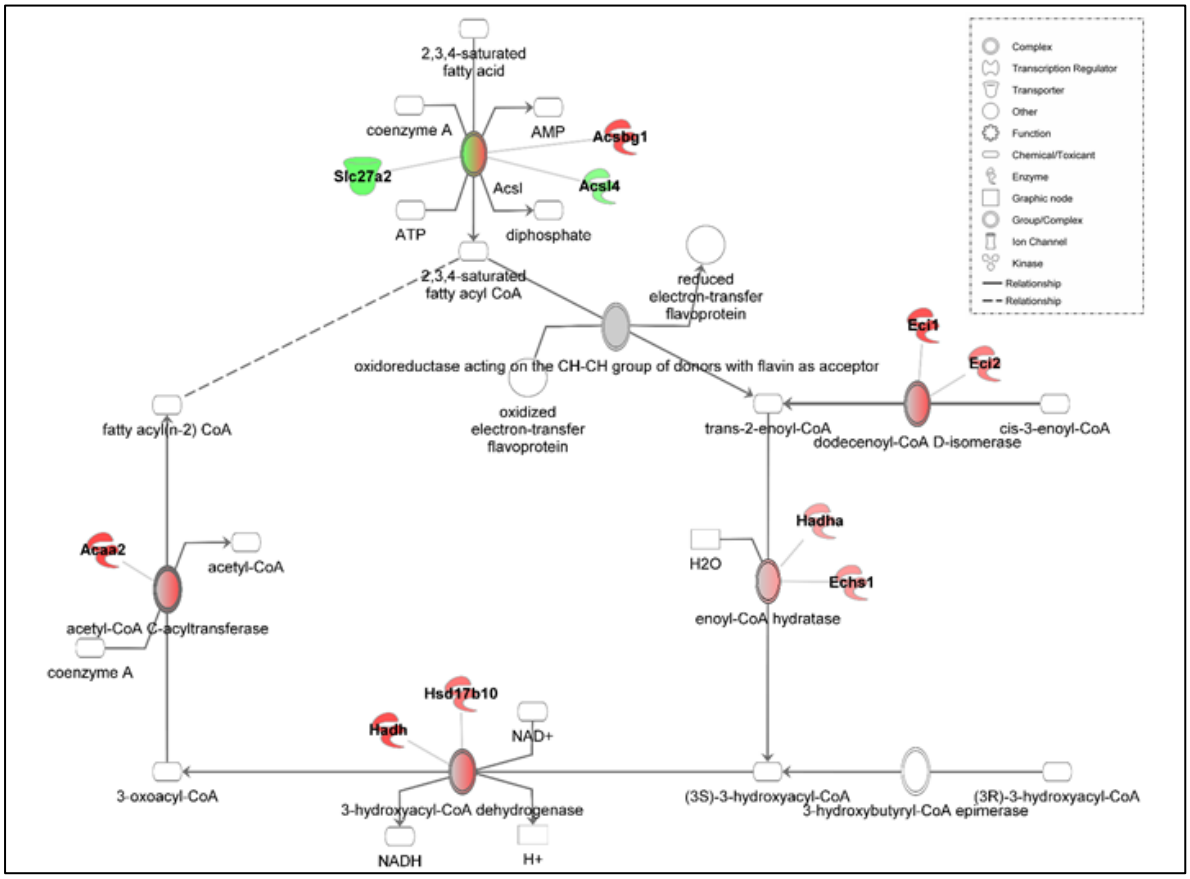

Supplementary Fig. 10 *Der1* cortex gene dysregulation within the 'Fatty acid β-oxidation I' canonical pathway. Pathway impairment was predicted by IPA based on gene dysregulation at the whole gene level using DESeq2 data. Double outlines indicate enzyme complexes. To provide additional information, genes encoding relevant dysregulated enzymes and a transporter have been added to the pathway using the IPA 'Build' tool. Colour intensity represents strength of gene expression change, with graded colour within double outlined symbols representing overall direction of change within protein complexes. green, downregulated; red, upregulated

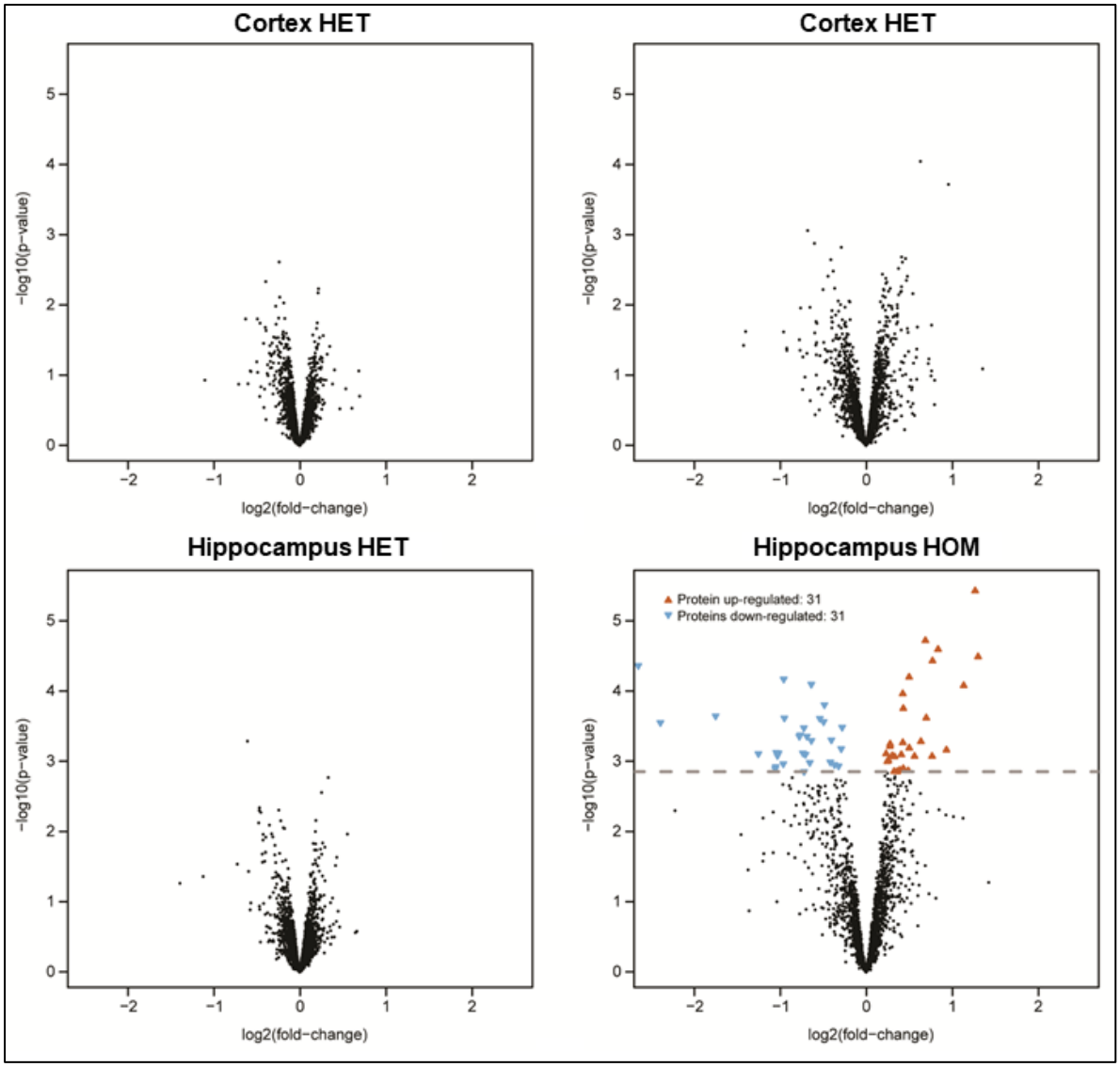

Supplementary Fig. 11 Volcano plots showing differentially expressed synaptosomes proteins in comparisons between *Der1* mice and wild-type controls. No significant differences were found after multiple testing correction in cortex from heterozygous and homozygous *Der1* mice, nor in hippocampus from heterozygous *Der1* mice. In hippocampus from homozygous *Der1* mice, 62 proteins were found to be significantly dysregulated (FDR adjusted p-value ≤ 0.05) as indicated by the coloured dots above the dashed line.

References

1. Malavasi ELV, Economides KD, Grunewald E, Makedonopoulou P, Gautier P, Mackie S *et al.* DISC1 regulates N-methyl-D-aspartate receptor dynamics: abnormalities induced by a Disc1 mutation modelling a translocation linked to major mental illness. *Transl Psychiatry* 2018; **8**(1)**:** 184.

2. Jenkinson M, Beckmann CF, Behrens TE, Woolrich MW, Smith SM. Fsl. *NeuroImage* 2012; **62**(2)**:** 782-790.

3. Avants BB, Tustison NJ, Song G, Cook PA, Klein A, Gee JC. A reproducible evaluation of ANTs similarity metric performance in brain image registration. *NeuroImage* 2011; **54**(3)**:** 2033-2044.

4. Richetto J, Chesters R, Cattaneo A, Labouesse MA, Gutierrez AMC, Wood TC *et al.* Genome-Wide Transcriptional Profiling and Structural Magnetic Resonance Imaging in the Maternal Immune Activation Model of Neurodevelopmental Disorders. *Cereb Cortex* 2017; **27**(6)**:** 3397-3413.

5. Wood TC, Simmons C, Hurley SA, Vernon AC, Torres J, Dell'Acqua F *et al.* Whole-brain ex-vivo quantitative MRI of the cuprizone mouse model. *PeerJ* 2016; **4:** e2632.

6. Tustison NJ, Avants BB, Cook PA, Zheng Y, Egan A, Yushkevich PA *et al.* N4ITK: improved N3 bias correction. *IEEE Trans Med Imaging* 2010; **29**(6)**:** 1310-1320.

7. Dorr AE, Lerch JP, Spring S, Kabani N, Henkelman RM. High resolution three-dimensional brain atlas using an average magnetic resonance image of 40 adult C57Bl/6J mice. *NeuroImage* 2008; **42**(1)**:** 60-69.

8. Avants BB, Yushkevich P, Pluta J, Minkoff D, Korczykowski M, Detre J *et al.* The optimal template effect in hippocampus studies of diseased populations. *NeuroImage* 2010; **49**(3)**:** 2457-2466.

9. Paxinos G, Franklin KBJ. The mouse brain in stereotaxic co-ordinates. 4 edn. Elsevier Academic Press: Amsterdam, The Netherlands, 2013.

10. Jiang H, Lei R, Ding SW, Zhu S. Skewer: a fast and accurate adapter trimmer for next-generation sequencing paired-end reads. *BMC Bioinformatics* 2014; **15:** 182.

11. Dobin A, Davis CA, Schlesinger F, Drenkow J, Zaleski C, Jha S *et al.* STAR: ultrafast universal RNA-seq aligner. *Bioinformatics (Oxford, England)* 2013; **29**(1)**:** 15-21.

12. Anders S, Pyl PT, Huber W. HTSeq--a Python framework to work with high-throughput sequencing data. *Bioinformatics (Oxford, England)* 2015; **31**(2)**:** 166-169.

13. Love MI, Huber W, Anders S. Moderated estimation of fold change and dispersion for RNA-seq data with DESeq2. *Genome biology* 2014; **15**(12)**:** 550.

14. Anders S, Reyes A, Huber W. Detecting differential usage of exons from RNA-seq data. *Genome Res* 2012; **22**(10)**:** 2008-2017.

15. Skene NG, Bryois J, Bakken TE, Breen G, Crowley JJ, Gaspar HA *et al.* Genetic identification of brain cell types underlying schizophrenia. *Nature genetics* 2018; **50**(6)**:** 825-833.

16. Newman AM, Liu CL, Green MR, Gentles AJ, Feng W, Xu Y *et al.* Robust enumeration of cell subsets from tissue expression profiles. *Nat Methods* 2015; **12**(5)**:** 453-457.

17. Pandya NJ, Koopmans F, Slotman JA, Paliukhovich I, Houtsmuller AB, Smit AB *et al.* Correlation profiling of brain sub-cellular proteomes reveals co-assembly of synaptic proteins and subcellular distribution. *Sci Rep* 2017; **7**(1)**:** 12107.

18. Koopmans F, Pandya NJ, Franke SK, Phillippens I, Paliukhovich I, Li KW *et al.* Comparative Hippocampal Synaptic Proteomes of Rodents and Primates: Differences in Neuroplasticity-Related Proteins. *Front Mol Neurosci* 2018; **11:** 364.

19. He E, Lozano MAG, Stringer S, Watanabe K, Sakamoto K, den Oudsten F *et al.* MIR137 schizophrenia-associated locus controls synaptic function by regulating synaptogenesis, synapse maturation and synaptic transmission. *Human molecular genetics* 2018; **27**(11)**:** 1879-1891.

20. Bruderer R, Bernhardt OM, Gandhi T, Miladinovic SM, Cheng LY, Messner S *et al.* Extending the limits of quantitative proteome profiling with data-independent acquisition and application to acetaminophen-treated three-dimensional liver microtissues. *Mol Cell Proteomics* 2015; **14**(5)**:** 1400-1410.

21. Koopmans F, van Nierop P, Andres-Alonso M, Byrnes A, Cijsouw T, Coba MP *et al.* SynGO: An Evidence-Based, Expert-Curated Knowledge Base for the Synapse. *Neuron* 2019; **103**(2)**:** 217-234 e214.

22. Martel MA, Ryan TJ, Bell KF, Fowler JH, McMahon A, Al-Mubarak B *et al.* The subtype of GluN2 C-terminal domain determines the response to excitotoxic insults. *Neuron* 2012; **74**(3)**:** 543-556.

23. McKay S, Ryan TJ, McQueen J, Indersmitten T, Marwick KFM, Hasel P *et al.* The Developmental Shift of NMDA Receptor Composition Proceeds Independently of GluN2 Subunit-Specific GluN2 C-Terminal Sequences. *Cell Rep* 2018; **25**(4)**:** 841-851 e844.

24. Kammers K, Cole RN, Tiengwe C, Ruczinski I. Detecting Significant Changes in Protein Abundance. *EuPA Open Proteom* 2015; **7:** 11-19.

25. Smyth GK, Michaud J, Scott HS. Use of within-array replicate spots for assessing differential expression in microarray experiments. *Bioinformatics (Oxford, England)* 2005; **21**(9)**:** 2067-2075.

26. Vasistha NA, Johnstone M, Barton SK, Mayerl SE, Thangaraj Selvaraj B, Thomson PA *et al.* Familial t(1;11) translocation is associated with disruption of white matter structural integrity and oligodendrocyte-myelin dysfunction. *Molecular psychiatry* 2019.

27. Ji B, Higa KK, Kim M, Zhou L, Young JW, Geyer MA *et al.* Inhibition of protein translation by the DISC1-Boymaw fusion gene from a Scottish family with major psychiatric disorders. *Human molecular genetics* 2014; **23**(21)**:** 5683-5705.

28. Eykelenboom JE, Briggs GJ, Bradshaw NJ, Soares DC, Ogawa F, Christie S *et al.* A t(1;11) translocation linked to schizophrenia and affective disorders gives rise to aberrant chimeric DISC1 transcripts that encode structurally altered, deleterious mitochondrial proteins. *Human molecular genetics* 2012; **21**(15)**:** 3374-3386.

29. Kuroda K, Yamada S, Tanaka M, Iizuka M, Yano H, Mori D *et al.* Behavioral alterations associated with targeted disruption of exons 2 and 3 of the Disc1 gene in the mouse. *Human molecular genetics* 2011; **20**(23)**:** 4666-4683.

30. Umeda K, Iritani S, Fujishiro H, Sekiguchi H, Torii Y, Habuchi C *et al.* Immunohistochemical evaluation of the GABAergic neuronal system in the prefrontal cortex of a DISC1 knockout mouse model of schizophrenia. *Synapse* 2016; **70**(12)**:** 508-518.

31. Nakai T, Nagai T, Wang R, Yamada S, Kuroda K, Kaibuchi K *et al.* Alterations of GABAergic and dopaminergic systems in mutant mice with disruption of exons 2 and 3 of the Disc1 gene. *Neurochemistry international* 2014; **74:** 74-83.

32. Iritani S, Sekiguchi H, Habuchi C, Torii Y, Kuroda K, Kaibuchi K *et al.* Catecholaminergic neuronal network dysfunction in the frontal lobe of a genetic mouse model of schizophrenia. *Acta Neuropsychiatr* 2016; **28**(2)**:** 117-123.

33. Tsuboi D, Kuroda K, Tanaka M, Namba T, Iizuka Y, Taya S *et al.* Disrupted-in-schizophrenia 1 regulates transport of ITPR1 mRNA for synaptic plasticity. *Nature neuroscience* 2015; **18**(5)**:** 698-707.

34. Tang W, Thevathasan JV, Lin Q, Lim KB, Kuroda K, Kaibuchi K *et al.* Stimulation of Synaptic Vesicle Exocytosis by the Mental Disease Gene DISC1 is Mediated by N-Type Voltage-Gated Calcium Channels. *Front Synaptic Neurosci* 2016; **8:** 15.

35. Shahani N, Seshadri S, Jaaro-Peled H, Ishizuka K, Hirota-Tsuyada Y, Wang Q *et al.* DISC1 regulates trafficking and processing of APP and Abeta generation. *Molecular psychiatry* 2015; **20**(7)**:** 874-879.

36. Delevich K, Jaaro-Peled H, Penzo M, Sawa A, Li B. Parvalbumin Interneuron Dysfunction in a Thalamo-Prefrontal Cortical Circuit in Disc1 Locus Impairment Mice. *eNeuro* 2020; **7**(2).

37. Shen S, Lang B, Nakamoto C, Zhang F, Pu J, Kuan SL *et al.* Schizophrenia-related neural and behavioral phenotypes in transgenic mice expressing truncated Disc1. *J Neurosci* 2008; **28**(43)**:** 10893-10904.

38. Dawson N, Kurihara M, Thomson DM, Winchester CL, McVie A, Hedde JR *et al.* Altered functional brain network connectivity and glutamate system function in transgenic mice expressing truncated Disrupted-in-Schizophrenia 1. *Transl Psychiatry* 2015; **5:** e569.

39. Booth CA, Brown JT, Randall AD. Neurophysiological modification of CA1 pyramidal neurons in a transgenic mouse expressing a truncated form of disrupted-in-schizophrenia 1. *Eur J Neurosci* 2014; **39**(7)**:** 1074-1090.

40. Pletnikov MV, Ayhan Y, Nikolskaia O, Xu Y, Ovanesov MV, Huang H *et al.* Inducible expression of mutant human DISC1 in mice is associated with brain and behavioral abnormalities reminiscent of schizophrenia. *Molecular psychiatry* 2008; **13**(2)**:** 173-186, 115.

41. Ayhan Y, Abazyan B, Nomura J, Kim R, Ladenheim B, Krasnova IN *et al.* Differential effects of prenatal and postnatal expressions of mutant human DISC1 on neurobehavioral phenotypes in transgenic mice: evidence for neurodevelopmental origin of major psychiatric disorders. *Molecular psychiatry* 2011; **16**(3)**:** 293-306.

42. Katsel P, Tan W, Abazyan B, Davis KL, Ross C, Pletnikov MV *et al.* Expression of mutant human DISC1 in mice supports abnormalities in differentiation of oligodendrocytes. *Schizophr Res* 2011; **130**(1-3)**:** 238-249.

43. Katsel P, Fam P, Tan W, Khan S, Yang C, Jouroukhin Y *et al.* Overexpression of Truncated Human DISC1 Induces Appearance of Hindbrain Oligodendroglia in the Forebrain During Development. *Schizophrenia bulletin* 2018; **44**(3)**:** 515-524.

44. Pogorelov VM, Nomura J, Kim J, Kannan G, Ayhan Y, Yang C *et al.* Mutant DISC1 affects methamphetamine-induced sensitization and conditioned place preference: a comorbidity model. *Neuropharmacology* 2012; **62**(3)**:** 1242-1251.

45. Abazyan B, Nomura J, Kannan G, Ishizuka K, Tamashiro KL, Nucifora F *et al.* Prenatal interaction of mutant DISC1 and immune activation produces adult psychopathology. *Biological psychiatry* 2010; **68**(12)**:** 1172-1181.

46. Kim J, Horti AG, Mathews WB, Pogorelov V, Valentine H, Brasic JR *et al.* Quantitative Multi-modal Brain Autoradiography of Glutamatergic, Dopaminergic, Cannabinoid, and Nicotinic Receptors in Mutant Disrupted-In-Schizophrenia-1 (DISC1) Mice. *Mol Imaging Biol* 2015; **17**(3)**:** 355-363.

47. Xia M, Zhu S, Shevelkin A, Ross CA, Pletnikov M. DISC1, astrocytes and neuronal maturation: a possible mechanistic link with implications for mental disorders. *Journal of neurochemistry* 2016; **138**(4)**:** 518-524.

48. Holley SM, Wang EA, Cepeda C, Jentsch JD, Ross CA, Pletnikov MV *et al.* Frontal cortical synaptic communication is abnormal in Disc1 genetic mouse models of schizophrenia. *Schizophr Res* 2013; **146**(1-3)**:** 264-272.

49. Xia M, Broek JA, Jouroukhin Y, Schoenfelder J, Abazyan S, Jaaro-Peled H *et al.* Cell Type-Specific Effects of Mutant DISC1: A Proteomics Study. *Mol Neuropsychiatry* 2016; **2**(1)**:** 28-36.

50. Hikida T, Jaaro-Peled H, Seshadri S, Oishi K, Hookway C, Kong S *et al.* Dominant-negative DISC1 transgenic mice display schizophrenia-associated phenotypes detected by measures translatable to humans. *Proceedings of the National Academy of Sciences of the United States of America* 2007; **104**(36)**:** 14501-14506.

51. Altimus C, Harrold J, Jaaro-Peled H, Sawa A, Foster DJ. Disordered ripples are a common feature of genetically distinct mouse models relevant to schizophrenia. *Mol Neuropsychiatry* 2015; **1**(1)**:** 52-59.

52. Cardarelli RA, Martin R, Jaaro-Peled H, Sawa A, Powell EM, O'Donnell P. Dominant-Negative DISC1 Alters the Dopaminergic Modulation of Inhibitory Interneurons in the Mouse Prefrontal Cortex. *Mol Neuropsychiatry* 2018; **4**(1)**:** 20-29.

53. Niwa M, Jaaro-Peled H, Tankou S, Seshadri S, Hikida T, Matsumoto Y *et al.* Adolescent stress-induced epigenetic control of dopaminergic neurons via glucocorticoids. *Science (New York, NY* 2013; **339**(6117)**:** 335-339.

54. Deng D, Jian C, Lei L, Zhou Y, McSweeney C, Dong F *et al.* A prenatal interruption of DISC1 function in the brain exhibits a lasting impact on adult behaviors, brain metabolism, and interneuron development. *Oncotarget* 2017; **8**(49)**:** 84798-84817.

55. Koike H, Arguello PA, Kvajo M, Karayiorgou M, Gogos JA. Disc1 is mutated in the 129S6/SvEv strain and modulates working memory in mice. *Proceedings of the National Academy of Sciences of the United States of America* 2006; **103**(10)**:** 3693-3697.

56. Kvajo M, McKellar H, Arguello PA, Drew LJ, Moore H, MacDermott AB *et al.* A mutation in mouse Disc1 that models a schizophrenia risk allele leads to specific alterations in neuronal architecture and cognition. *Proceedings of the National Academy of Sciences of the United States of America* 2008; **105**(19)**:** 7076-7081.

57. Lepagnol-Bestel AM, Kvajo M, Karayiorgou M, Simonneau M, Gogos JA. A Disc1 mutation differentially affects neurites and spines in hippocampal and cortical neurons. *Molecular and cellular neurosciences* 2013; **54:** 84-92.

58. Kvajo M, McKellar H, Drew LJ, Lepagnol-Bestel AM, Xiao L, Levy RJ *et al.* Altered axonal targeting and short-term plasticity in the hippocampus of Disc1 mutant mice. *Proceedings of the National Academy of Sciences of the United States of America* 2011; **108**(49)**:** E1349-1358.

59. Crabtree GW, Sun Z, Kvajo M, Broek JA, Fenelon K, McKellar H *et al.* Alteration of Neuronal Excitability and Short-Term Synaptic Plasticity in the Prefrontal Cortex of a Mouse Model of Mental Illness. *J Neurosci* 2017; **37**(15)**:** 4158-4180.